Journal of Materials Processing Tech. 292 (2021) 117062

Contents lists available at ScienceDirect

Journal of Materials Processing Tech.

journal homepage: www.elsevier.com/locate/jmatprotec

Limits to making L-shape ring profiles without ring growth

Christopher John Cleaver [a,*], Johannes Lohmar [b], Saeed Tamimi [c]

[a] Department of Engineering, University of Cambridge, Trumpington Street, CB2 1PZ, United Kingdom
[b] Institute of Metal Forming, RWTH Aachen University, Intzestraße 10, 52072, Aachen, Germany
[c] Advanced Forming Research Centre (AFRC), University of Strathclyde, Glasgow, United Kingdom

ARTICLE INFO

Associate Editor: Dr Jian Cao

Keywords:
Ring rolling
Net shape forming
Process limits
Thermomechanical FEM

ABSTRACT

A novel ring rolling process is proposed to flexibly produce shaped rings without circumferential ring growth, potentially saving material and energy as well as reducing upstream and downstream processing requirements. In this paper, six circumferential constraint rolls are used constrain circumferential growth and enable L-shape profiles to be developed through axial material flow, via a compressive hoop stress. Process limits were studied in 22 experiments on lead rings and a set of axisymmetric thermally coupled simulations on a high value engineering material, Inconel 718. Profile depths of 75 % of the original wall thickness were achieved in a range of rings and operating conditions, and material savings of up to 60 % demonstrated over rectilinear rolling. There was no evidence of cracking or void formation, unlike processes where under-deformed regions are stretched circumferentially and are vulnerable to cracking. In several cases a non-circular ring shape developed, limiting the achievable profile depth especially for small wall thicknesses, large reductions in thickness per pass, or large profile heights. The constraint roll forces when this 'collapse' occurs was studied and an upper bound predicted by a plastic hinge model. The thermal simulations showed that in all except 4 cases reheats would be required to keep within safe temperature bounds, thus suggesting an optimum reduction in thickness per pass to avoid both excessive cooling and collapse.

1. Industrial importance of L-shaped profiled rings

Seamless rings are widely used for rotating machinery and fluid transfer applications in engineering equipment in various industrial sectors including aerospace, electricity generation, oil and gas, and marine. Worldwide, seamless rings – produced by ring rolling - made up 6 % of forged products in 2018, as shown in Fig. 1. Production volumes are generally on the rise: sales grew by 93 % in USA in the decade to 2014.

The final applications for seamless rings require high product performance in terms of mechanical strength, fatigue life and often high-temperature performance and corrosion resistance. Customers translate these requirements into detailed specifications on microstructure and mechanical properties.

The final components often also have a complex cross-sectional shape, as shown in Fig. 1c. However, in many cases the established supply chain is for ring rollers to supply semi-finished products that are larger than the component, often with a rectangular cross-section. The component geometry is then produced by machining, resulting in large volumes of scrapped material. There are clear benefits to producing rings closer to their net-shape by ring rolling, including cost-saving, avoiding waste, reducing both downstream processing and material handling requirements, and near to net-shape 'profiled' rings have been produced for a number of years (e.g. as described by Marczinski, 1984).

However, it remains a significant industrial challenge to configure a ring rolling process to produce an L-shaped profile, especially if the required profile is deep and the stock material is not already shaped, as will be discussed next.

2. State of the art: producing profiled components by ring rolling

This section explores what is known about the technology of producing profiled rings, focusing on the challenges of making L-shapes.

It is helpful to provide some terminology to describe the shape of the final profiled rings; we use three key non-dimensional figures of merit; the profile depth Ψ, the profile feature height Γ, and the ring slenderness, Λ.

* Corresponding author.
E-mail address: cjc82@cam.ac.uk (C.J. Cleaver).

https://doi.org/10.1016/j.jmatprotec.2021.117062
Received 21 August 2020; Received in revised form 15 January 2021; Accepted 17 January 2021
Available online 20 January 2021
0924-0136/© 2021 The Authors. Published by Elsevier B.V. This is an open access article under the CC BY license (http://creativecommons.org/licenses/by/4.0/).

$$\Psi = \frac{t}{T} \quad (1)$$

$$\Gamma = \frac{h}{H} \quad (2)$$

$$\Lambda = \frac{IR}{T} \quad (3)$$

where T is the maximum wall thickness, H is the height, IR is the inner radius, t is the difference between the maximum wall thickness and the profiled feature wall thickness, and h is the height of the profiled feature – all indicated in Fig. 2c for an L-shape ring.

Hawkyard and Moussa (1984), were amongst the first to discuss the central difficulty with producing shaped rings which is that if we start with a simple rectangular cross-section blank, then given that volume is conserved some form of axial flow of material is required to produce a shape. However, with a conventional tooling set-up, only the wall thickness is directly controlled and there is little or no means to ensure the right amount of axial flow happens.

For example, Hawkyard and Moussa investigated making an L-shaped profile from an initially rectangular billet. The tooling and set up were as illustrated in Fig. 2a. For the process to work as intended (ideal result) then volume conservation requires a large amount of axial flow of material from initial region 1a into the final region 2b. In practice they found that not enough axial flow occurs, so the lower region is stretched, and it is 'underfilled'. A profile depth Ψ of approximately 33 % was achieved whereas the fully formed profile would have had Ψ = 50 %. The shape of the profile also differed somewhat from ideal.

Hawkyard and Moussa found that if the blank is already shaped – see Fig. 2b - so that Regions 1a' and 1b' contains the same volume of material as Regions 2a and 2b respectively, there was an improvement in profile filling. In this case a larger profile depth of 38 % was achieved. Further improvements to the final shape were possible if the upper region of the blank was tapered.

Similarly, Qian and Hua (2010) compared four blank design options producing an outer-L shape ring, through FE simulation and experimental trials. They also concluded that the optimal blank is the one that pre-distributes the material in the same proportion as the target product. This, they concede, requires a more complex process route for blank production such as blocker-type forging or die forging. One such process route was outlined by Oh et al. (2019), see Fig. 3a. The method uses a large shaped lower die and conical punch; in likelihood both would have to be custom-made for each part in question. Their study showed that even with a shaped blank, minor shape defects such as a groove in the lower axial surface can occur. These were reduced by small tooling and blank design changes.

Deeper profiles might still be produced *without* requiring a shaped blank if the circumferential growth of the ring is constrained in some way. Several innovative approaches have been investigated in literature involving partial contact and by using additional tooling.

Salimi (1988) proposed a rocking mandrel that contacts only a portion of the ring's inner radial surface at any point – see top of Fig. 4a [I}. In principle, the region of the ring not in contact with the tool would act as a constraint to circumferential flow, and hence improve profile filling. The construction of a rocking mandrel is not trivial, and Salimi ran a series of experiments to demonstrate the principle by interrupting the rolling process and manually adjusting a tapered mandrel. Profile filling improved by approximately 70 %.

Allwood et al. (2005) introduced the concept of 'incremental' ring rolling, which uses a rolling tool shorter than the full height of the ring to produce a profiled ring through a series of thickness reductions at different heights – see Fig. 4a [II]. However, the pattern of deformation caused by these indentations is difficult to predict a-priori, and blank design and path planning is challenging. Tiedemann et al. (2007) went some way to providing an empirical model for the axial flow of material 'out' of the region behind the short tool and claimed some success in producing complex profiles.

A second approach by which researchers have looked to influence profile formation is to use additional tooling to constrain circumferential growth. Qian et al. (2013) proposed a process they name combined cross rolling to produce a C-shaped ring with a deep inner groove, see Fig. 4b [III]. In this, two rolls were placed approximately 120° apart opposite the roll gap, and these play a role in restricting circumferential growth and enabling spread. Qian et al.'s simulations suggests an almost five-fold increase in the profile depth achieved compared to rolling without cross-rolls, with Ψ reaching 53 %. The approach was demonstrated experimentally. Qian et al. (2013) discuss the limits to combined cross rolling; postulating there is a limit to the height of groove that can be produced and that changes to machine set-up would be required to produce bigger rings. The method seems to be reliant on the ring's rigidity against collapsing in-plane, and the experiment was done on a thick-walled ring of slenderness, Λ, 1.2, much lower than other studies. It is likely there is also a limit on the slenderness of the rings that can be produced.

To avoid just such a problem, and to produce highly complex profiles, some researchers have investigated using a complete closed die around the ring to constrain it. Kluge et al. (1997) demonstrated how an external die could be used to produce a conical shaped component, see Fig. 4b[IV]; this shaped ring had both a large profile depth, with average Ψ of about 60 %, and large profile height Γ of about 70 %. Han et al. (2014) showed how a similar approach can be used to produce a ring that is much taller than the initial blank. The material saving possibility is quite large and the approach – of

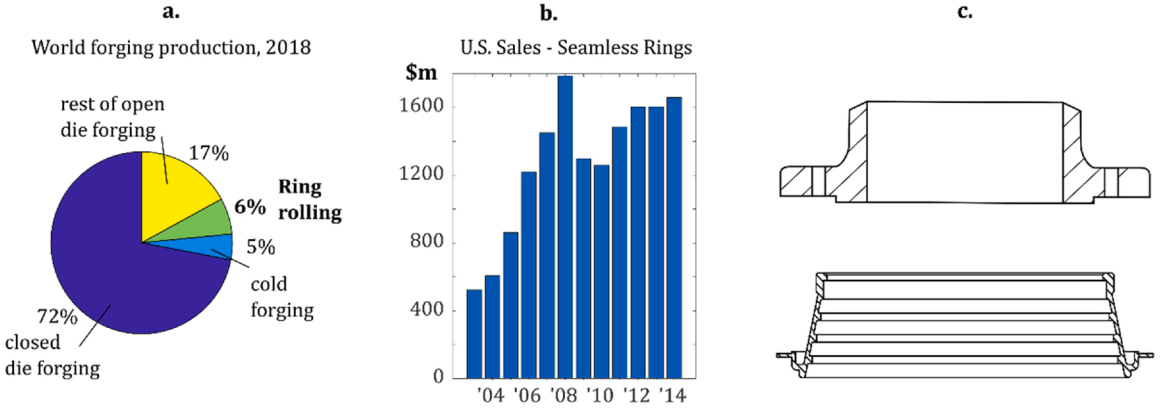

Fig. 1. a. Worldwide production of forgings, 2018 by production mass (Euroforge, 2020) **b.** Sales of seamless rings in USA (Forging Industry Association, 2015) **c.** Cross-section views of example annular components produced by ring rolling.

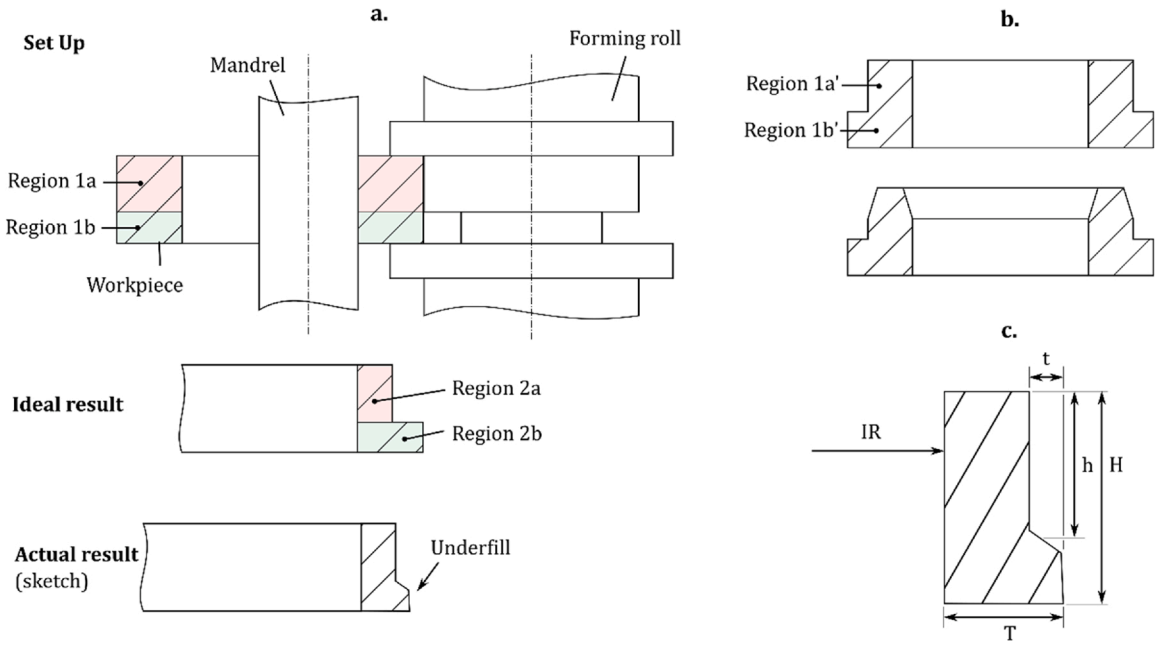

Fig. 2. Production of an outer L shape profile with **a.** a rectangular blank **b.** a shaped blank **c.** definition of variables used to define a profile feature.

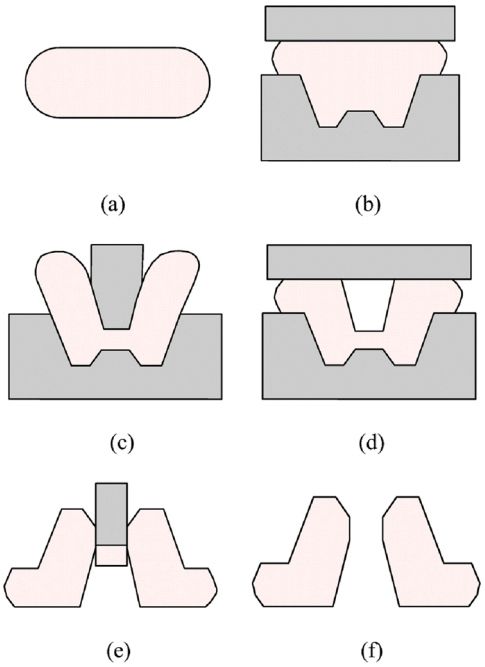

Fig. 3. Blank production method for L-Section rolling (Oh et al., 2019) Image reproduced with permission of copyright holder.

completely constraining circumferential flow by a certain point in the process - appears to be a reliable way to enforce the axial flow needed to produce a given profile. However, the tooling itself is very expensive and difficult to produce.

To some extent, Cleaver and Allwood (2017a), (2017b)) combined the two approaches shown in Fig. 4a–c [V]. A set of six circumferential constraint rolls, and two axial constraint rolls were introduced to influence the flow of material in partial contact rolling – see Fig. 4c. This set-up was used to produce an inner L-shape ring, and the additional constraints enabled a relatively deep profile ($\Psi = 50\%$) to be produced with fewer corrective passes. Here, the six circumferential constraint rolls resisted circumferential flow but still allowed the ring to grow in circumference. In a later investigation on conical rings Cleaver and Allwood (2017b) demonstrated that in certain circumstances the force applied by the six constraints is sufficient to prevent ring growth completely, in the same manner as a closed die such as used by Kluge et al.(1997) and Han et al. (2014); however, this approach has not yet been systematically studied for L-shapes.

A key consideration for process set-ups that use additional tooling to constrain the ring is the influence of this tooling on the ring temperature distribution. Increasing the process time, or the area of the ring in contact with tooling could increase the amount of cooling and make a process infeasible. For instance, when using an external die, Kluge et al. (1997) discuss the need to avoid forming thin-walled features until late on in the process. Meanwhile Lohmar et al. (2020) found that trebling the constraint rolls has a moderate influence on the cooling rate, potentially limiting the applicability of the process introduced by Cleaver and Allwood (2017a), (2017b)).

Furthermore, a second concern for methods that produce highly profiled parts from rectangular blanks is the possibility of ductile damage due to the large differences in thickness strain applied, and the possibility of stretching under deformed 'dead-zones'. For example, Moussa (1981) showed how edge cracks can develop in the under-deformed flange of a profiled, cold-rolled aluminium ring. Furthermore, Wang et al. (2016) demonstrated that a slow ring growth rate in hot ring rolling – i.e. small reductions in thickness per pass - results in increased ductile damage. The former could potentially be avoided if the ring is not allowed to grow in circumference.

Table 1 summarises the approaches to profile ring rolling reviewed so far, firstly those that use shaped blanks to enable profile filling, and those that use other methods such as partial contact with the ring, and additional constraining tools. In all cases the material saving is modest compared to producing a rectangular cross-section ring that envelopes the profile – a maximum of 45 % when a full external die was used, and 35 % otherwise. This is because to save a large amount of material both a large profile depth *and* height are required. Across all the studies, the profile feature height Γ ranges from 30 to 75%, whilst the profile depth Ψ ranges from 28 to 71%. Since they are approximately multiplicative, the material savings are somewhat smaller and may be further reduced by errors in precise form. The slenderness ranges from just 1.2 to a maximum of 19, although in all except one case this number is less than 10.

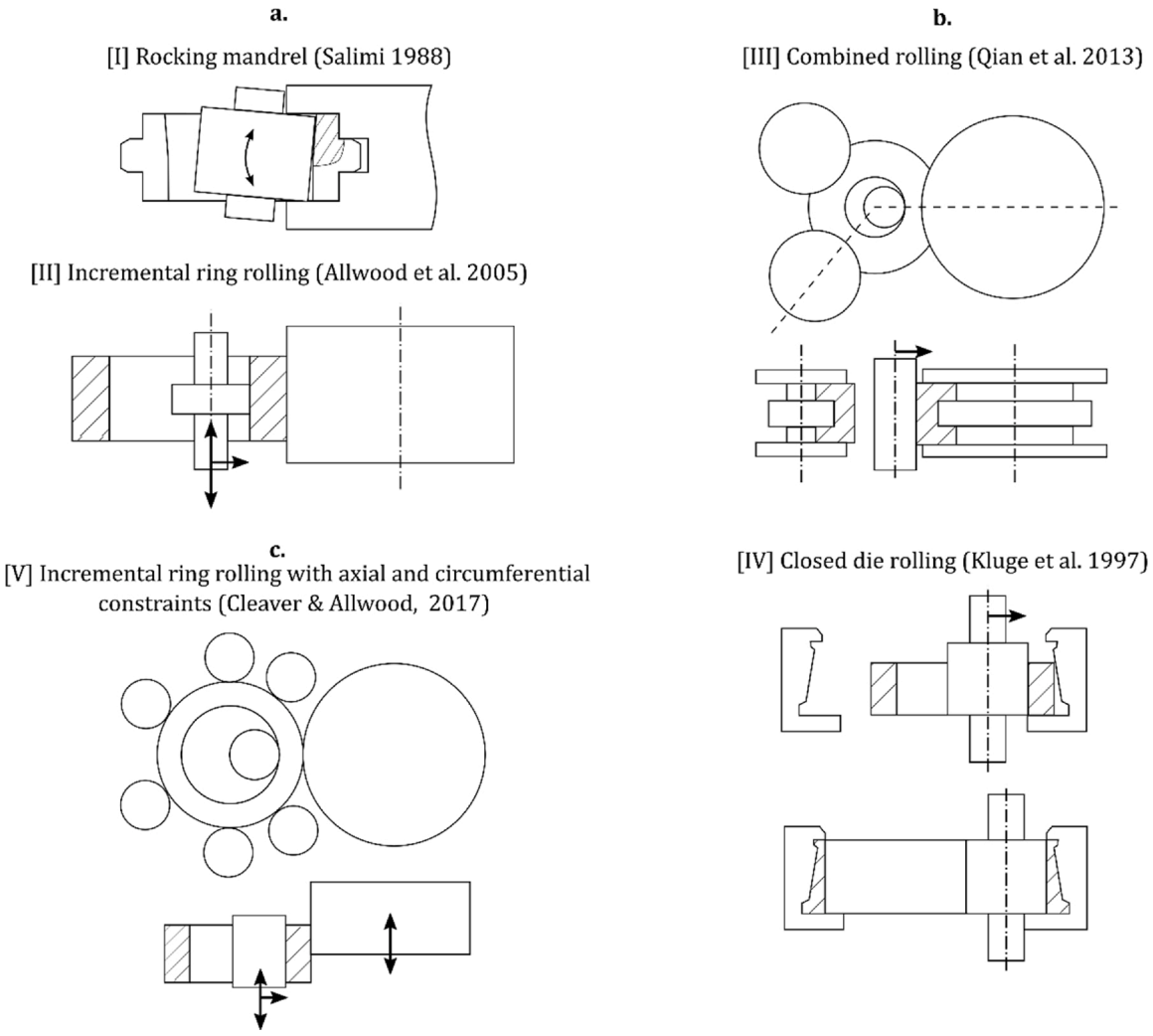

Fig. 4. Novel approaches to improve profile formation **a.** using partial ring contact **b.** using additional tooling to constrain circumferential growth **c.** using both a. and b.

Table 1
Summary of approaches to profile ring rolling selected from the literature.

Study	Profile shape	Extra Constraint	Blank Type	Profile depth, Ψ	Profile height, Γ	Approx. material saving	Slender-ness, Λ
Hawkyard and Moussa (1984)	Outer L	None	Shaped	38 %	70 %	28 %	9.4
Qian and Hua (2010)	Outer L	None	Shaped	57 %	50 %	30 %	5.6
Oh et al. (2019)	Outer L	None	Shaped	71 %	46 %	35 %	1.2
Hawkyard and Moussa (1984)	Outer L	None	Rectangular	33 %	70 %	23 %	19
Salimi (1988)	Inner T	Partial contact	Rectangular	28 %	75 %	21 %	4.2
Kluge et al. (1997)	Conical	Full ext. die	Rectangular	60 %	72 %	45 %	2.9
Qian et al. (2013)	Outer C	2 circ. rolls	Rectangular	53 %	31 %	19 %	1.2
Cleaver and Allwood (2017a)	Inner L	6 circ. rolls	Rectangular	50 %	62 %	21 %	7.3
			Max.	71 %	75 %	45 %	19
			Min.	28 %	31 %	19 %	1.2

The range of investigations carried out into profile ring rolling have been reviewed, including several specifically into L-shape rolling. Some promising approaches to this challenging problem exist including blank optimization, partial contact on the ring, and the use of specialized constraint tools, although only the former is known to be commonly used in industry.

Despite the multitude of approaches, Table 1 showed that most have achieved only relatively modest material savings. Furthermore, most studies considered only one target product and have not sought to define the limits to the range of shapes that may be produced by a given method. This is important, since as briefly discussed with reference to combined cross-rolling (Qian et al., 2013), each method is likely to have limitations on the range of profile height, depth, and the ring slender-ness amongst other properties.

This paper focuses on the industrially important class of L-shape rings, and using the tooling set-up proposed by Cleaver and Allwood (2017a), (2017b) asks what are the mechanical and thermal limits to shaping an initially rectangular blank, without ring growth and without using a large external die around the ring?

3. Concept for profiling without ring growth

A novel concept for making profiled rings without ring growth is introduced, made possible by the tooling arrangement on the University of Cambridge Incremental Ring Rolling machine. The proposed shaping process is first described, and then key process limits are anticipated. The principle for the process is that local contact with six constraining rolls generates a large enough circumferential stress in the ring to influence the forming conditions in the main radial roll gap, forcing the ring grow in height rather than circumferentially.

To produce an L-shaped ring, an intermediate product of the correct volume and outer diameter, and with a rectangular cross-section, is first made. This is then transformed into an L-shape - see Fig. 5a.

The shaping process is achieved by rolling to reduce a portion of the ring's wall thickness whilst using the constraining rolls to prevent ring growth. The powered forming roll tool is lifted so that it initially contacts a fraction h/H_0 of the ring surface as shown in Fig. 5a. The region it contacts will become the 'thin wall' of the L, whilst the region below will become the thick 'flange'. The inner mandrel contacts the full inner radial surface. The six constraining rolls around the circumference are used to control the circumferential growth of the ring; i.e. to prevent extension of the workpiece in the rolling direction. All rolls described overlap the ring's upper axial surface, whilst the ring is supported on its lower axial surface. As the rolling process proceeds, the forming roll rotates whilst the radial roll gap is closed and the 'thin-wall' region becomes thinner. These constraints force the material to spread axially, while the ring gets taller and the flange retains roughly its original thickness.

In the rest of the paper four non-dimensional parameters are used to describe the main process variables, these are: ψ, the profile depth; γ, the profile height; λ, the slenderness of the initial blank; and δ, the reduction in thickness per revolution. The first three parameters, ψ, ν and λ which take lower case Greek characters, relate respectively to Ψ, Γ, and Λ that describe the *final* shape, as introduced in Eqs. 1–3.

$$\psi = \frac{\Delta T}{T_0} \tag{4}$$

$$\gamma = \left(\frac{h}{H}\right)_0 \tag{5}$$

$$\lambda = \left(\frac{IR}{T}\right)_0 \tag{6}$$

$$\delta = \frac{\Delta T_i}{T_i} \tag{7}$$

where ΔT is the total closure of the radial roll gap, T_0 is the initial wall thickness, h_0 is the height of the ring initially in contact with the outer forming roll, H_0 is the initial ring height and IR_0 is the initial inner radius, ΔT_i is the current difference in ingoing and outgoing wall thickness, and T_i is the current wall thickness.

There are several options for achieving the broad concept of 'no ring growth'[1], three are detailed in Fig. 5b. Firstly, the constraint rolls could simply be held stationary at the initial outer radius, OR_0, so that the outer diameter of the thin-wall region does not change (I). This approach results in a small increase in the average ring diameter. Or, the constraint rolls could be moved inwards by a fraction, *x,* of the closure of the radial roll gap to maintain the same average diameter throughout (II). Finally, they could move inwards at the same rate as the closure of the radial roll gap so that there is no change to the ring's inner radius (III). Preliminary experiments suggested that the difference in outcome between these approaches is very slight, and so (I) was used in this paper for its simplicity.

[1] 'Ring growth' is used as shorthand for circumferential growth, or equivalently, diameter growth

3.1. Process principle

The principle of how the constraining rolls prevent ring growth is now explored, followed by a description of the expected deformation pattern.

The six constraining rolls are thought to prevent ring growth by applying an additional compressive 'back pressure', σ_b, to the material in the radial roll bite, see Fig. 6a. This combined with the constraint imposed by the under deformed 'flange' region, makes it favourable for material in the radial roll bite to spread axially rather than extend circumferentially.

The back pressure required to enforce axial flow, $\sigma_{b\text{-}ax}$ is likely to be a fraction of the saturation flow stress, $\widetilde{\sigma_f}$. This is due to both stress superposition - the radial tools have already brought the material to the current flow stress - and the presence of the flange region not in direct contact with the outer tool. Fig. 6b explores how the back pressure might develop through the initial stages of a trial. In the very early stages of the process the back pressure, σ_b, increases rapidly. At this stage, the workpiece is extending slightly, causing it to bulge outwards elastically between each constraining roll. This generates reaction forces F_i at each roll and therefore back pressure. At some point the back pressure reaches the 'axial flow pressure', $\sigma_{b\text{-}ax}$, the material flows axially only, and so the back pressure does not increase further.

The relationship between the force at the constraining rolls, and the back pressure can be estimated by Eq. 8, by a force balance in the direction aligned with σ_b, assuming the pressures at the roll bite and opposite it are equal:

$$\sigma_b = \frac{1}{2A^{'}} \sum_{i=4,5,6} F_i \sin\alpha_i \tag{8}$$

Where $A^{'}$ is the cross-sectional area of the workpiece under the projection of the forming roll (i.e. $A^{'} = h * t$, where h, t are as shown in Fig. 5) and α_i is the angular position of the roll.

An L profile is thus expected to emerge through axial flow of material *transverse* to the rolling direction. However, it is not known how far the constraints will force material into the flange, or how far it will result in an overall increase in height of the thin-wall region – see Fig. 7a. Assuming both thin-wall region and the flange remain rectangular in cross-section, then it is possible to show the trade-off between these effects as a function of χ, the proportion of the material volume displaced that flows into the flange:

$$\chi = \frac{V_{flange} - U_{flange}}{U_{thin} - V^{'}_{thin}} \tag{9}$$

where U_{flange} and V_{flange} are the initial and final volumes of the flange region, U_{thin} is the initial volume of the thin-walled region and $V^{'}_{thin}$ is the final volume of the thin-walled region up to the original height of the ring, dashed in Fig. 7a.

Fig. 7b shows that if χ is zero, i.e. there is no flow of material into the flange, the flange would reduce in thickness because of the slight increase in average radius. An appeal to the relative difficulty of each flow 'route' suggests that whilst χ is unlikely to be exactly zero, it will be small and that height growth will dominate. The value of, and the assumption that the volumes remain broadly rectangular in shape will be revisited in the results – Figs. 19 & 20 .

3.2. Anticipated process limits

There are several potential limits to the efficacy of this new ring rolling process. This study explores three: plastic collapse in the plane of the ring, ductile damage, and excessive temperature loss in hot processing.

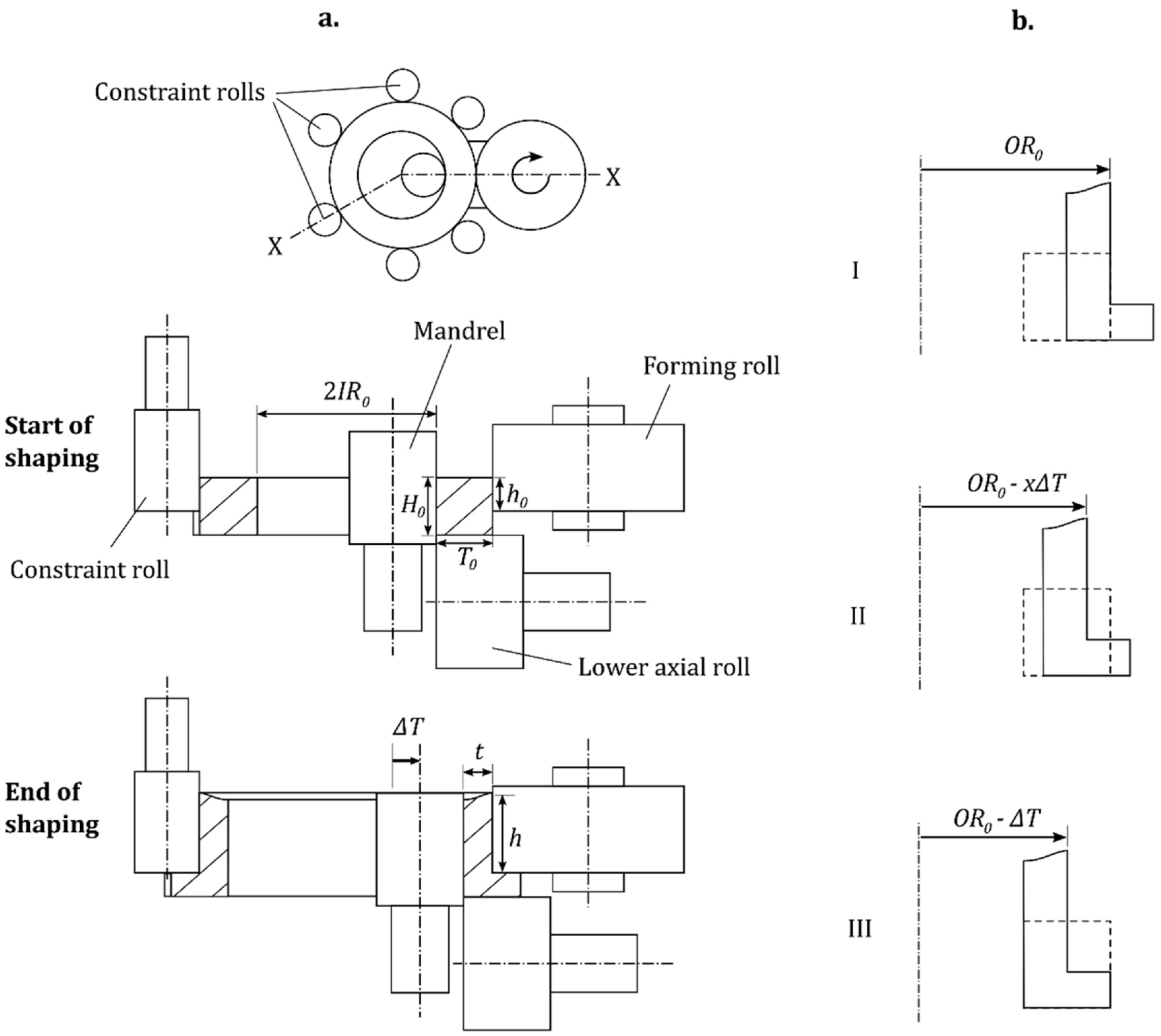

Fig. 5. **a.** Set-up for producing outer L-shape profiles without ring growth **b.** Options for constraint roll motion.

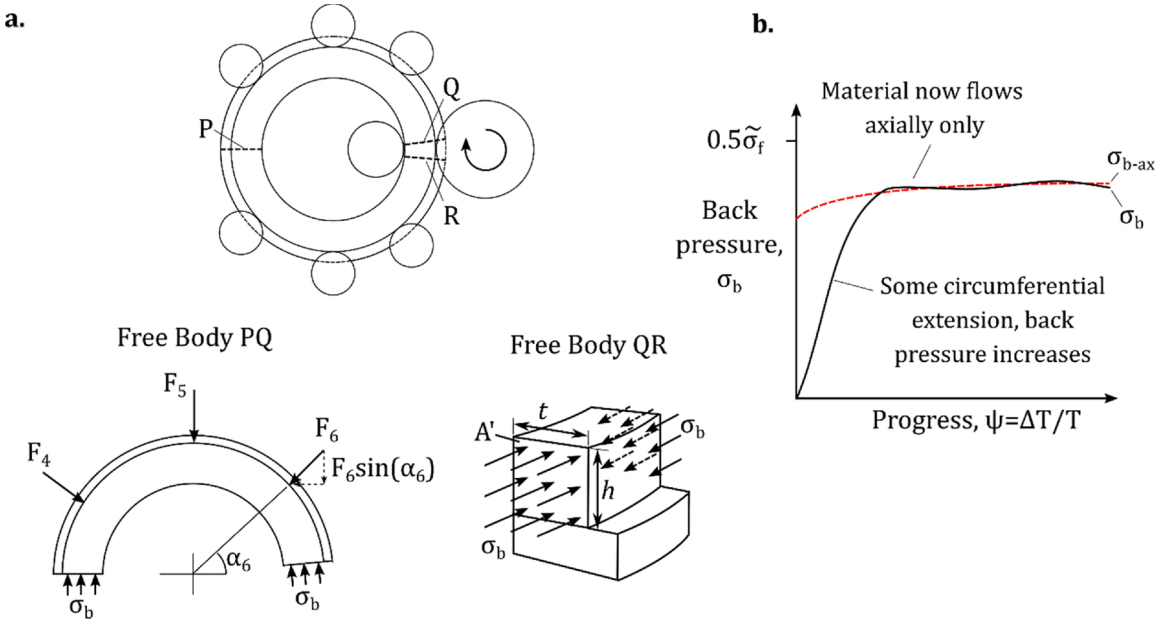

Fig. 6. **a** Free body cuts P,Q,R applied to the ring to show the back pressure on the radial roll bite region **b** Schematic evolution of back pressure against reduction in wall thickness.

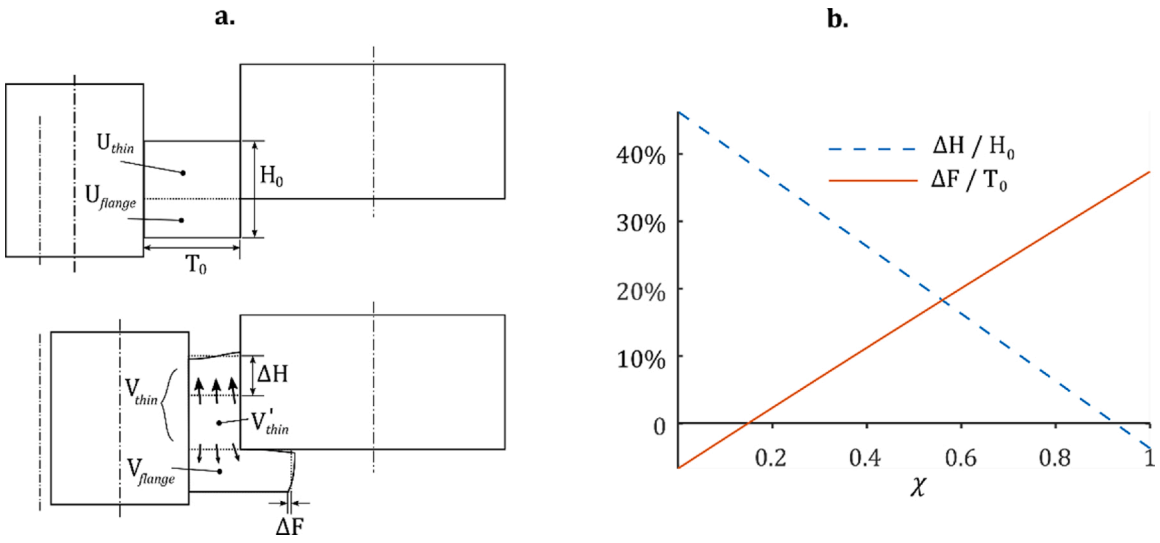

Fig. 7. **a.** Material flow cartoon **b.** Average height growth vs. flange thickness growth as a function of χ, the proportion of displaced material entering the flange, for $\psi = 0.5$, $\gamma = 0.5$ and $\lambda = 6$, assuming volume conservation.

3.2.1. *Plastic collapse*

Previous work has shown that the ring can lose circularity when the constraint roll force that prevents ring growth is too large – we call this plastic collapse.

Cleaver (2017) showed that in the set-up where six constraint rolls are used around the ring there becomes a point where the ring loses circularity and 'collapses' when the constraint roll forces increase, as shown in Fig. 8a. A ring of rectangular cross-section was rolled, and collapse occurred when the force applied by the constraint rolls reached approximately 5 times the ratio of the plastic moment to the ring radius. The plastic moment is the moment in bending which causes the entire cross-section to reach the flow stress and plastically deform. A pattern of plastic hinges form, which allows the ring to grow circumferentially in between the constraint rolls, until the experiment is halted. In comparison, when two guide rolls were used a much smaller force was needed to cause a loss in circularity - approximately 0.3−0.5 times the same ratio.

This agrees with Li et al.'s (2008) analysis which sought to determine the force that can be sustained when two guide rolls are used before the ring loses circularity. They found that the guide roll force should not exceed a factor (less than unity) of the force that would first generate yielding assuming the ring is cantilevered from the roll-bite.

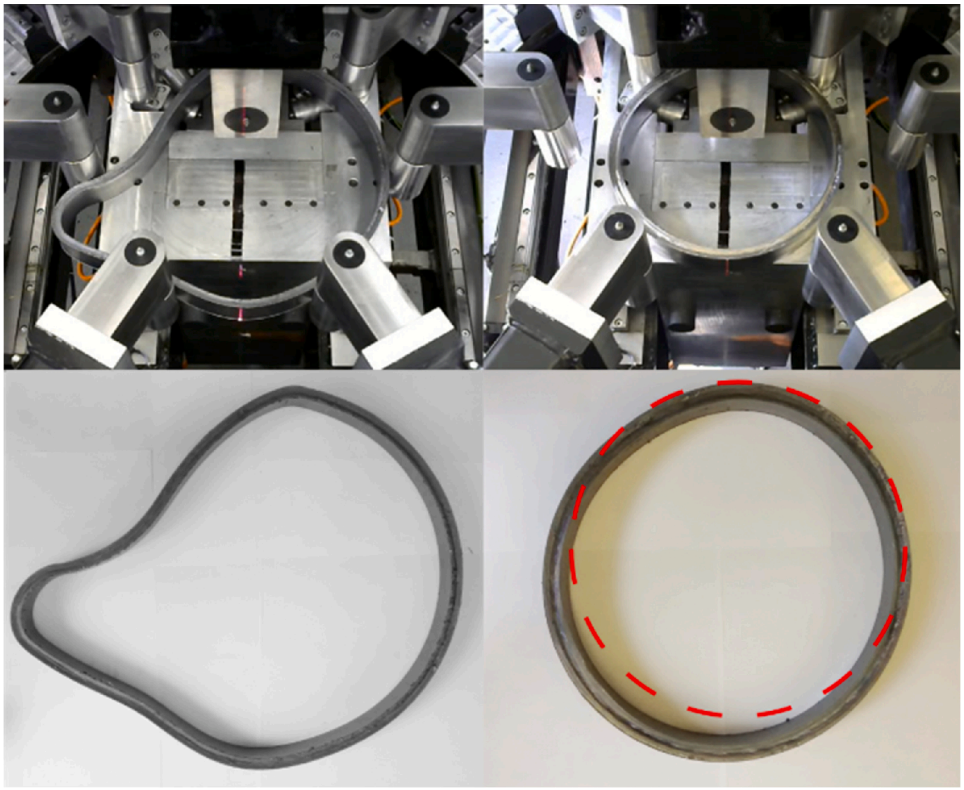

Fig. 8. Test to establish maximum constraint roll force in radial ring rolling **a.** (left) six constraint rolls **b.** (right) conventional set-up with 2 guide rolls, (Cleaver, 2017). Image reproduced with permission of copyright holder.

This collapse load can equivalently be thought of as a collapse back pressure, σ_{b-col}. This is plotted on Fig. 9a, extending the axes previously used in Fig. 6b. The collapse pressure, σ_{b-col}, might initially be higher than the current back pressure and the process proceeds 'safely'. However, as the ring changes shape its capacity to withstand the back pressure might reduce and instead of continuing to flow axially, it is possible for a series of plastic hinges to form causing a loss in circularity. Thereafter the back pressure oscillates as the non-circular ring exerts an oscillating pressure on the constraint rolls. It is difficult to predict the eventual ring shape, but it might resemble that shown in Fig. 9b.

To predict the collapse an estimate for both the axial flow pressure, $\sigma_{b\text{-}ax}$, and the collapse pressure, $\sigma_{\text{b-col}}$ is needed. This paper next presents an upper bound for $\sigma_{\text{b-col}}$ using a plastic hinge model.

Applying the upper bound method, we assume a compatible deformation pattern as shown in Fig. 9b. There are plastic hinges at the point of contact with each roll, and in the centre of each arc between rolls, fourteen in all. Considering the pattern of hinges adjacent to one constraint roll, Fig. 9c, the roll force, F_i, to generate this deformation can be calculated by virtual work. If the force, F_i, moves a small distance x, this generates rotations at hinges A, B and C of ϕ, 2ϕ and ϕ respectively. By equating distances perpendicular to OC, where O is the centre of the ring:

$$\frac{x\ sin(\beta)}{2R\ sin\left(\frac{\beta}{2}\right)} = \cos\left(\frac{\beta}{2}\right) - \cos\left(\frac{\beta}{2}+\phi\right) \tag{10}$$

where R is the average radius and β is the half angular spacing between rolls. Expanding the right term and using the small angle approximations $\cos\phi \approx 1$ and $\sin\phi \approx \phi$ we have:

$$\phi = \frac{x\ sin(\beta)}{2R\ sin^2(\beta/2)} \tag{11}$$

Equating the external work done to the internal work to rotate the hinges A, B, C then:

$$F_i x = 4M_p\phi \tag{12}$$

$$F_i = \frac{4M_p\ sin(\beta)}{2R\ sin^2(\beta/2)} \tag{13}$$

Where M_p is the plastic moment. For constant flow stress, M_p is the product of the flow stress and the plastic section modulus, Z_p. The critical back pressure can be calculated by applying Eq. 8.

3.2.2. Ductile damage

Ductile damage – such as voids and micro-cracks – leading to failure by fracture might also limit the ring shaping process. Given the high degree of shaping anticipated, different areas in the workpiece will experience very different process conditions. Whereas the thin-walled region (Fig. 6a) will almost certainly experience compressive radial stress due to the direct effect of the tooling, the flange region is not directly contacted on both inner and outer radial surfaces. Thus, the flange is more likely to experience positive triaxiality, which has a well-established link to increased damage and ultimately failure (e.g. Garrison and Moody, 1987).

Indeed, in previous work where the ring grows in diameter the flange region has been shown to be vulnerable to failure by cracking (for example Moussa, 1981). It is not yet established to what extent the process proposed in this paper will overcome this vulnerability.

3.2.3. Thermal processing limits

Given the focus on material savings, a natural application for the novel process is high value engineering materials. Rolled rings in these high strength materials typically require hot processing and a key limiting factor will be the ability to keep the ring temperature within 'safe' processing bounds. This is a concern for many metals, but one of the most challenging high value engineering materials are Nickel based superalloys. Of these, a key alloy is Inconel 718, for which workpieces are typically heated to around 1030 °C in furnace, but temperatures below approximately 900 °C are to be avoided due to material becoming brittle and prone to damage (Thomas et al., 2006). This can be achieved by careful process planning and reheating the workpiece – producing a profiled ring made of a Nickel based superalloy typically involves several process stages (De Souza et al., 2003) – however, there is a practical limit to the number of reheats that are feasible due to their high cost in time and energy.

Lohmar et al. (2020) showed that for radial-only rolling, increasing the number of rolls in contact with the ring has a moderately negative effect on ring temperature. However, this could be mitigated by increasing the process speed, afforded by the additional stability the rolls bring. Therefore, it is of great interest to understand and estimate the reheat requirements for the shaping without ring growth process: will this be a limiting factor?

4. Methodology: experiments and FE on shaping without ring growth

This paper seeks to determine and understand limiting factors for a novel approach to L-shaping without ring growth. A series of 22 experiments on lead were carried out to investigate plastic collapse and ductile damage limits. In addition, a novel simplified Finite Element Analysis (FEA) approach was taken to investigate *thermal* processing limitations *only* for the high value material, Inconel 718. The 2-D approach allowed a corresponding set of 22 simulations to be carried out in a reasonable time. Two further 3-D FEA simulations were also

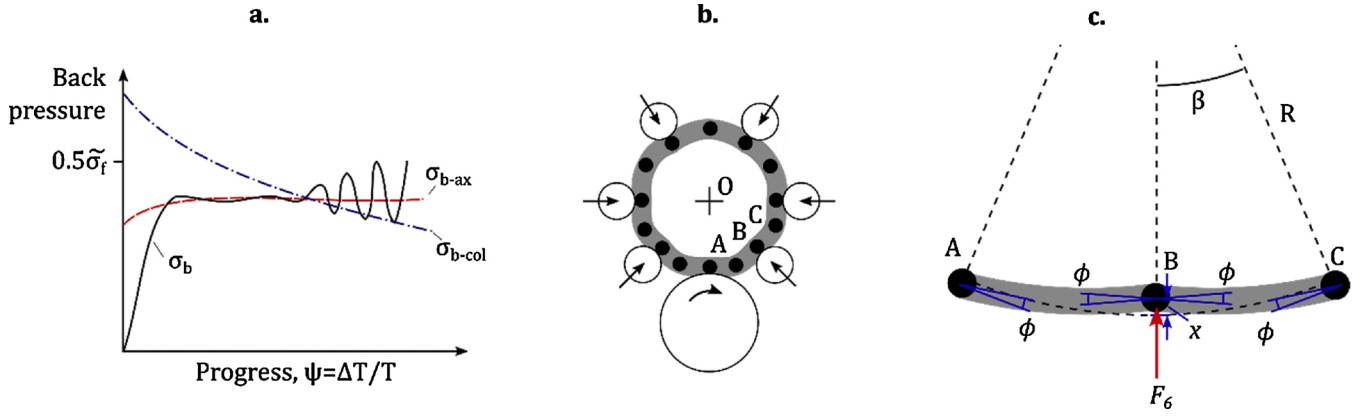

Fig. 9. a. Schematic evolution of back pressure when a collapse occurs **b.** Plastic hinge model to describe the collapse **c.** Kinematics of collapse around one constraint roll.

performed to explore the transferability of the lead results to Inconel 718. Details of the physical experiments and finite element simulations are given next, leading to an overall design of the investigations in this paper.

4.1. Physical experiments on the Cambridge Incremental Ring Rolling Machine

The physical experiments were carried out on the Cambridge Incremental Ring Rolling machine, shown in Fig. 10. The machine arrangement was shown in Fig. 5a, with six circumferential constraint rolls, a mandrel and forming roll that can each be repositioned vertically, and the option to apply an axial constraint on the ring, thus enabling shaping by partial contact as described in Section 2.

The limited force capacity of the machine necessitates use of a model material; lead was chosen for this since at room temperature it is above its recrystallisation point (−4 °C) and is generally representative of hot-working and rate-dependent metals. Whilst all of the limits to shaping will of course be somewhat material dependent a good deal of the results will be transferrable, especially the plastic collapse limit since it is likely that both the driving force for collapse and the structural resistance to it are equally linked to the flow stress of the material, and so almost independent of its actual value.

Cast billets were prepared, and these were pre-rolled by different amounts to provide three accurate and uniform starting workpiece shapes. Pre-rolling was done in the conventional manner to produce a rectangular section starting blank with the same outer diameter as the target product.

The shaping experiments were carried out using the tool arrangement in Fig. 5a. The mandrel moves horizontally towards the forming roll, whilst the other tools remain stationary. The required reduction in thickness is achieved by closing the gap with a constant speed over the course of each revolution, calculated assuming there is no slip between the forming roll and the workpiece.

For each experiment, the shaping process was continued until either the ring had visibly collapsed, or until a targeted reduction in thickness was achieved. Further details including roll sizes, and speeds common to all the experiments are given in Table 2.

The mandrel closure force was recorded from a load cell, whilst an indication of the constraint roll forces is available from motor current readings. The constraint forces were estimated from the motor current using the torque constant supplied by the motor manufacturer and assuming the efficiency is the same as the known value for the radial roll axis, 74 % (Cleaver, 2017). For the medium-wall and thin-walled rings the outer profile shape was recorded by an optical laser profile scanner; however, this data was not available for the thick-walled rings because the constraint roll blocks the image.

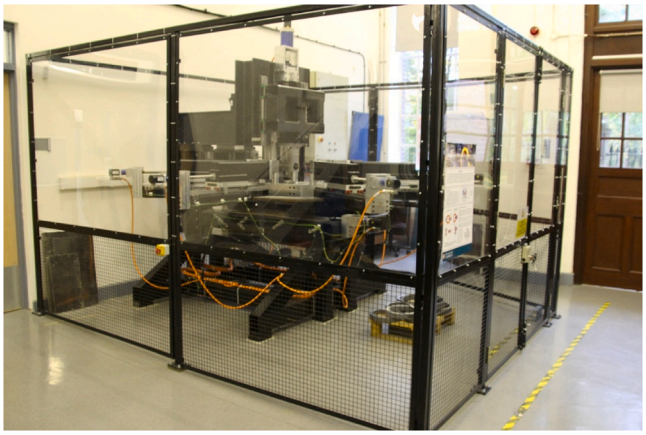

Fig. 10. Cambridge Incremental Ring Rolling Machine.

Table 2
Details of the experimental set-up.

Parameter	Value
Ring aspect ratio (H_0/T_0)	1
Forming roll surface speed	100 mm / s
Forming roll radius	100 mm
Mandrel radius	45 mm
Constraint roll radius	31 mm
Constraint roll number & locations	6 @ ±45°, ±90°, ±150° (rollbite is at 0°)
Ring initial wall thickness (T_0)	25.0 mm – Thick and Thin 29.4 mm – Medium

4.1.1. Ductile damage investigation - ultrasound testing

A range of options are typically available for ductile damage investigation including metallographic examination, X-ray tomography and scanning acoustic microscopy (SAM). The former proved infeasible due to difficulties with sample preparation and etching. Initial experiments also showed that the X-ray CT scanning was not suitable due to the high density of lead. However, SAM was found to be suitable for probing samples of depth up to around 3 mm, and this was used to investigate the existence and evolution of voids on a subset of the rings.

The SAM testing was carried out with a PVA TePla SAM 300. In this, sound pulses are sent into the sample and as they pass through the material, voids and any other types of defects focus the sound field. Reflected pulses are transformed into electromagnetic pulses which display as pixels whenever a defect of sufficiently large size is detected. Two shaped samples were studied alongside one representative as-cast specimen and one pre-rolled specimen. To achieve the highest defect sensitivity, a 110 MHz probe was selected, capable of probing to a depth of around 3 mm. This set up was able to detect voids or defects larger than 15 microns. The images provided were from scans over 150 × 80 mm for the samples with 2000 pixels in the X axis and a 1:1 X-Y Ratio.

Due to the limited depth that could be probed, segments of the rings were further cut into two sections: 'horizontal' and 'vertical' as shown in green and blue in Fig. 10, using a waterjet cutter. For the as-cast and pre-rolled samples, with rectangular cross-section (Fig. 11a), the horizontal section was cut 3 mm from the top axial surface, and a 3 mm thick vertical section was taken 5 mm from the rough-cut end of the segment. For the shaped samples (Fig. 11b) the horizontal slice was cut 3 mm from the top surface of the flange part. The vertical section which has an L-shape, including wall and flange areas, is again taken 5 mm from the rough cut end. The scanning process produces a series of images for layers of increasing depth into the sample; the images presented in the results are from the middle layer approximately 1.5 mm into the sample.

4.2. Thermo-mechanical finite element simulation

This paper chooses to investigate the reheat requirements for the situation where the shaping without ring growth concept is applied to a commonly used Nickel-based superalloy, Inconel 718. This material was chosen due to the combination of its high value, and challenging thermal processing requirements: if material savings can indeed be achieved, they will be prized. This thermal limit alone is investigated using a novel simplified 2-D axisymmetric simulation approach, taking advantage of the high degree of constraint the ring experiences, and enabling simulation of 22 different shapes and radial reductions as set out in Section 4.3.

4.2.1. Simplified 2-D model to investigate reheat limit

The simplified 2-D axisymmetric model was used to investigate the *reheat limit*. The reasons for the simplification are twofold: Firstly 3-D FEA of the L-Shaping of rings using the shaping without ring growth approach is very difficult to implement due to the specific deformation pattern where a roll is 'biting into' the ring. Secondly, the mesh and explicit solver imply very small time steps that lead to a simulation time of more than two weeks per simulation with a mass scaling factor of 100

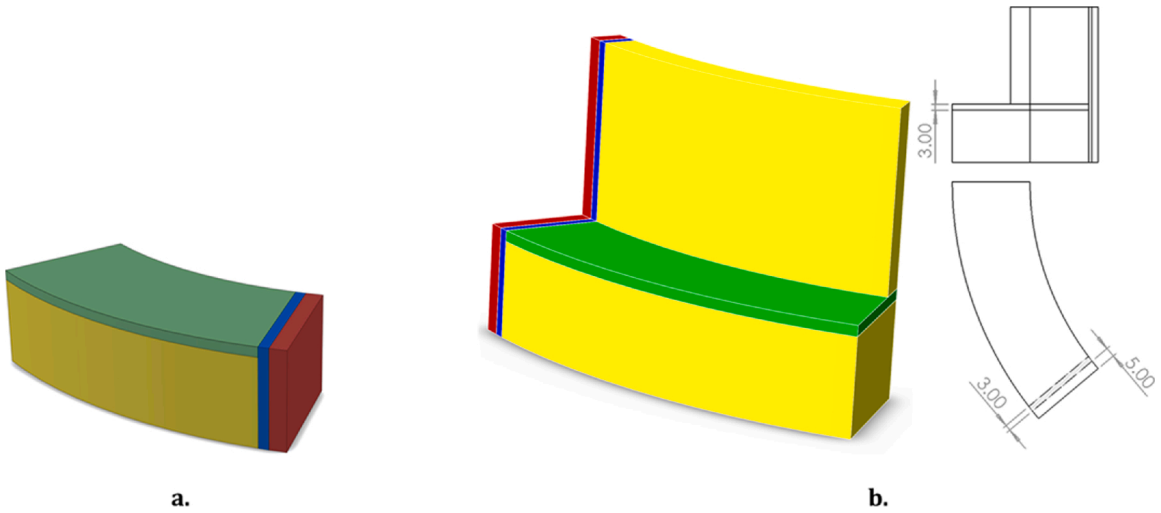

Fig. 11. Slicing process and samples for ultrasonic testing: **a.** as cast and pre-rolled **b.** shaped samples.

and thus do not allow for an extensive simulation study, whereas the 2-D approach took only 1–3 days per simulation with a mass scaling factor of 10.

In the 2-D model, implemented in ABAQUS finite element analysis software, the ring is modelled as an axisymmetric deformable body, see Fig. 12. The tools are modeled as isothermal rigid bodies. The initial heat, and subsequent reheats are modelled by setting/resetting the ring temperature to 1030 °C, making the reasonable assumption that the temperature is homogenous by the time the workpiece is ready to exit the furnace. An implicit 'Cooling' analysis step of duration 15 s is used to model the cooling during transfer from furnace to the machine; representative of typical practice for rings of this size.

Each revolution of the profile rolling process is modelled as follows: firstly, a radial reduction in wall thickness equivalent to the reduction in one pass through the roll bite is applied by moving the inner tool (representing the mandrel) towards the stationary outer tool (representing the combined effect of the forming roll, and the constraint rolls). This is modelled by a thermally coupled explicit 'Forming' analysis step. Conduction between the ring and the isothermal tools is considered together with radiation to the environment. Coulomb friction between tools and ring is used. This friction model is commonly used in ring rolling, since relative motion between these two bodies can occur (Zhou et al., 2010). A friction coefficient of 0.25 for the Inconel 718 to tool steel contact in hot ring rolling is applied in the present model which is in line with

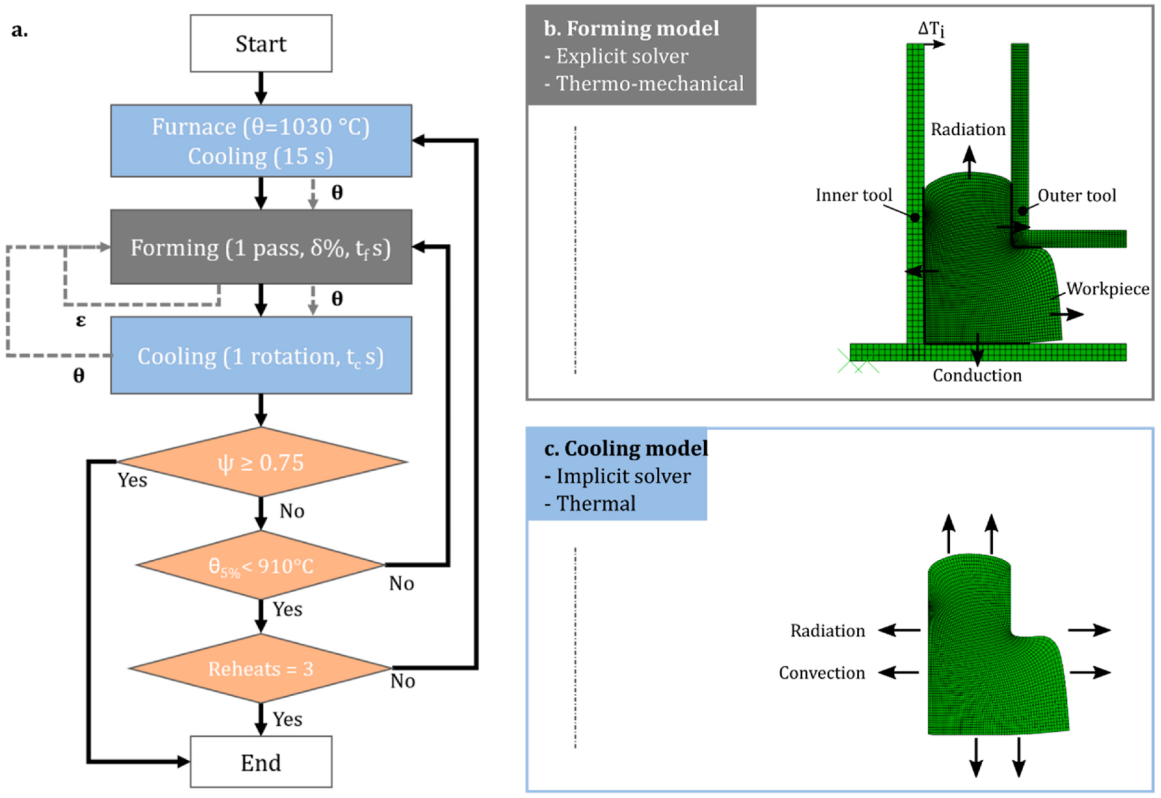

Fig. 12. Finite Element model details **a.** Flow chart of FE process including the coupling between 'Forming' and 'Cooling' models **b.** Forming model set up **c.** Cooling model set up.

previous work (Lohmar et al., 2020). To mitigate the risk of severe mesh distortion at the point where the roll is 'biting into' the ring the 'Arbitrary-Lagrangian-Eulerian' (ALE) simulation technique integrated into ABAQUS is applied. This dynamic remeshing approach reduces the element distortion throughout the 'Forming' step.

Then, an implicit 'Cooling' analysis step is used to represent the cooling experienced by each region of the ring after it leaves the roll bite and rotates through the remainder of a revolution. In this step, in addition to radiation, convection to the surrounding air is also considered. The temperature field, $\boldsymbol{\theta}$, is carried over between subsequent 'Forming' and 'Cooling' steps. Furthermore, the strain field, $\boldsymbol{\varepsilon}$, is transferred from each 'Forming' step to the next.

The material model is based on a tabulated flow stress data for Inconel 718 at 7 temperatures between 900−1100 °C, and 4 strain rates in the range 0.001−1/s, obtained from the literature (Medeiros et al., 2000). In Inconel 718, dynamic recrystallisation slows significantly below 900 °C and hard participates start to form, strongly reducing ductility, and so a lower limit is usually placed on forming temperature (Thomas et al., 2006). If the ring cools beyond these limits a reheat is necessary. To reflect this, at the end of each revolution a temperature check is performed: if more than 5% of the ring's cross-sectional area is below 910 °C, then a reheat is modelled.

The time for each forming step, t_f, was set to equal the expected duration of contact in the roll bite, using the method outlined by Koppers and Kopp (1992). The cooling step duration t_c is the remainder of the time expected to complete a ring revolution, t, quoted in Table 3. Unlike conventional rolling, the rotation time does not change throughout the process because the outer diameter remains constant. Further modelling details are given in Table 3.

4.2.2. 3-D model to investigate plastic collapse

To further explore the transferability of the lead experimental results on plastic collapse to Inconel 718, a high value engineering material, two 3-D Finite Element simulations were carried out also using ABAQUS software.

The ring is modelled as a 3-D deformable body using a mesh with element edge length of ~2 mm, as shown in Fig. 13. All rolling tools are modelled as rigid bodies with an isothermal temperature. The idle mandrel, the driven forming roll and the six constraint rolls have temperatures of 200 °C, 100 °C and 50 °C, respectively. A rolling table is modelled to provide additional support to the ring. Like in the 2-D axisymmetric simulations the ring has an initial temperature 1030 °C and again an implicit heat transfer step of duration 15 s is used to model the cooling during transfer from furnace to the machine.

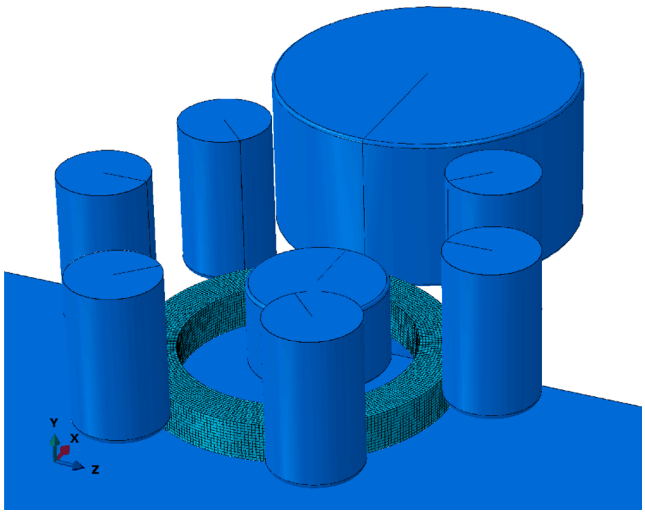

Fig. 13. 3-D FEA model set up.

To model the L-shape forming a thermally coupled explicit analysis is performed. The forming roll is offset from the base of the ring and rotates whilst the mandrel is moved inwards towards it, reducing the wall thickness of the upper region of the ring, and forcing the lower region under the forming roll to form a flange. To aid simulation stability, Coulomb friction with a coefficient of 0.3 is assumed only in between the ring and the forming roll and mandrel, respectively. The contact to the six constraint rolls and rolling table is assumed to be frictionless. Again, ALE is used to mitigate the risk of severe distortion of the ring's mesh. Throughout the simulation conduction between the ring and the isothermal rolls is considered together with radiation to the environment. All relevant interaction parameters are again given in Table 3.

4.2.3. Model verification

The 2-D axisymmetric model is being used to estimate the reheat requirements for this novel process in the absence of suitable equipment to roll high strength engineering materials. Given there is no experimental data to make a direct comparison to, a 2-D axisymmetric model of plain radial rolling was done also, for which experimental data and a verified 3-D simulation was available, as presented by Lohmar et al. (2020). For this, an emissivity of 0.9 was used to match the value used previously.

This comparison is shown in Fig. 14. The temperature profiles predicted by the models are similar: higher temperatures are seen in the centre of the ring, and these drop off towards the surfaces, and edges. The average temperature along the centre-line AB is 988 °C for the 2D simulation, compared to 1000 °C for the 3-D case (a 1.6 % difference), and along the upper surface CD, the average temperatures are 903 °C and 912 °C for 2-D and 3-D respectively (a 1% difference). The main cause of the difference seems to be dissipation: the 2-D simulation predicts significantly less plastic work in the regions of the ring near to the forming roll – see the distribution of plastic equivalent strain (PEEQ) – and so the 2-D simulation underpredicts the temperature in this region.

The dissipation discrepancy is largely because the 2-D simulation does not capture shear strains in the r-θ direction. Fig. 14 also plots the development through time of the average radial strain and r-θ shear strain along AB for both 2-D and 3-D simulations. The radial strains agree as expected. However, even though the absolute value of r-θ shear strain, only present in 3-D simulation, is relatively small, because of significant strain reversal (the peaks in r-θ strain) the accumulated shear strain is large, leading to a much higher PEEQ overall. Similar shear

Table 3
Details of the thermo-mechanical Finite Element models for L-shaped rings.

Parameter	2-D Axisymmetric	3-D	Reference
Forming roll surface speed	760 mm / s	760 mm / s	Lohmar et al. (2020)
Ring rotation time, t	0.82 s; 1.69 s; 2.26 s	0.82 s; 2.26 s	N/A
Forming time, t_f	0.0038 – 0.023 s	N/A	N/A
Mandrel temperature	200 °C	200 °C	Lohmar et al. (2020)
Forming roll temperature	100 °C	100 °C	Lohmar et al. (2020)
Contact heat transfer	9000 Wm^{-1} K^{-1}	9000 Wm^{-1} K^{-1}	Lu et al. (2017)
Convection heat transfer	5 Wm^{-1} K^{-1}	5 Wm^{-1} K^{-1}	Lu et al. (2017)
Emissivity	0.85	0.85	N/A
Dissipation	0.90	0.90	N/A
Flow stress	Tabulated flow stress at 900−1100 °C and 0.001−1/s strain rate		Medeiros et al. (2000)
Element type - Cooling model	DCAX4	DC3D8	N/A
Element type – Forming model	CAX4RT	C3D8RT	N/A
Workpiece element count	3,800 – 9,400	46,306; 139,256	N/A
Mass scaling	10	100	N/A

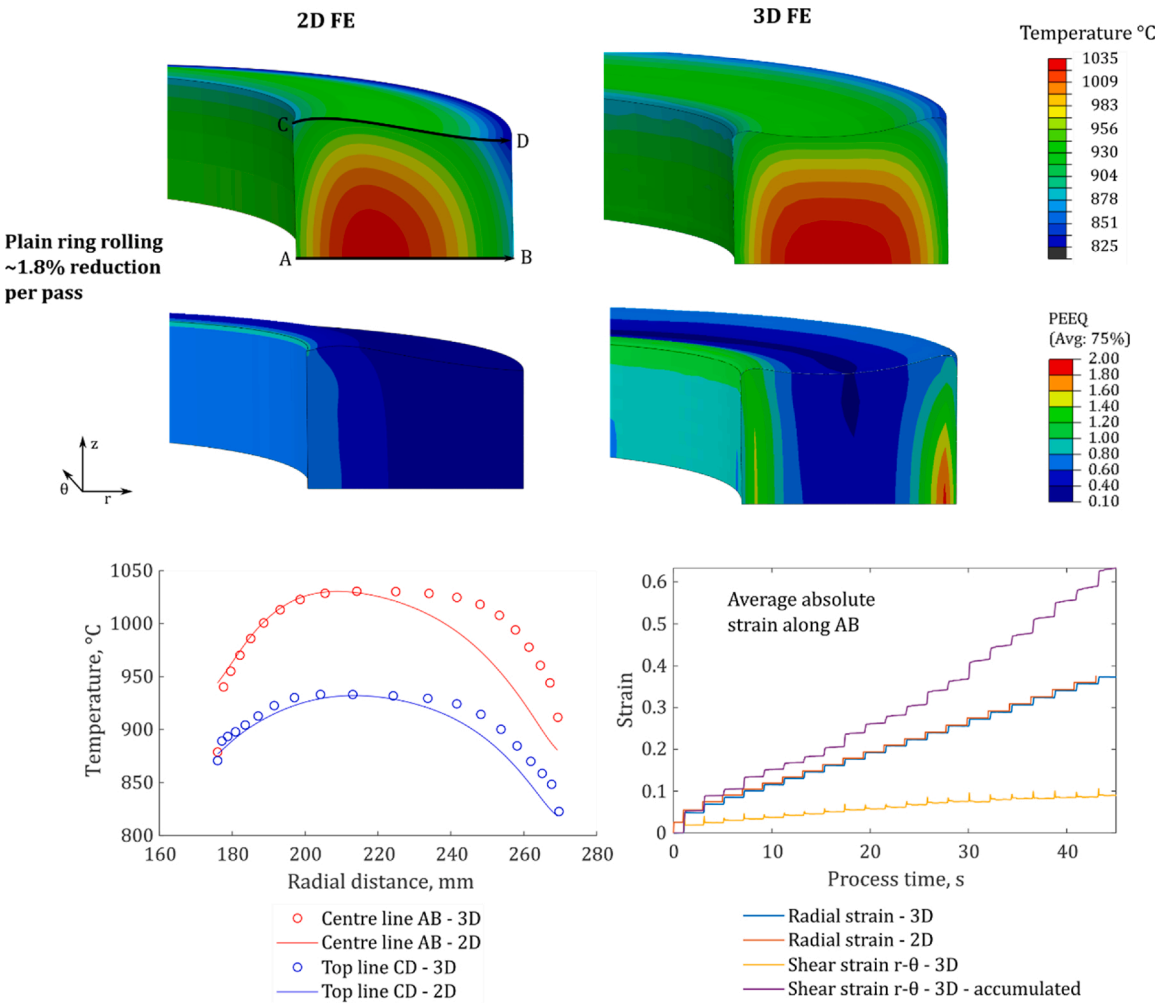

Fig. 14. Plain rolling of Inconel 718: 2-D axisymmetric FEM vs a verified 3-D FEM simulation.

strain reversals have been reported for plate rolling (Seuren et al., 2014). As a result, the 2-D simulation underpredicts heating due to plastic dissipation.

A further factor affecting model reliability is how far the 2-D model can predict the shape developed in the *profile* rolling process. Fig. 15 compares the 2-D simulation of Inconel 718 to the experimental results in lead. Whilst the overall shape is broadly similar, the 2D simulations occupy a different bounding box, or 'envelope'. For 2 % reduction per pass, the 2-D simulations show both less axial spread – the axial envelope is 15 % and 22 % smaller for the profile heights of 66 % and 33 % respectively – and reduced flange wall thickness - the radial envelope is 38 % and 6 % smaller for profile heights of 66 % and 33 %. For 12 % reduction per pass cases, the disparities are smaller: axial and radial discrepancies are within 8 % and 13 % respectively.

These are, in truth, some quite large discrepancies and there are several possible reasons for it. One issue appears to be a loss in volume in the simulation caused by the remeshing process. In the very worst case - $h/H = 66$ % and $\delta = 2$% per pass - the 2-D simulation was found to lose 21 % of its volume by the end of the process. However, the volume loss is much smaller for higher reductions per pass, and smaller profile heights: it is 4.2 % for the case $h/H = 66$ % and $\delta = 12$ % per pass, and for $h/H = 33$ %, the volume loss is 6.7 % and 0.7 % for reductions of $\delta = 2$ % and 12 % respectively. Future work could look to optimize the ALE setup to minimize this discrepancy. The lead ring itself may have had a slightly larger volume than expected: the pre-rolled rings were found to be about 0.4 mm (1.6 %) taller due to deflection of the machine during the radial-axial pre-rolling. It is also clear that the 2-D simulation does not capture errors in form such as the non-uniform height growth in the thin-walled region and underfill in the flange. Finally, the lead experiments only approximately model the hot working of Inconel 718 and so may themselves be a poor indicator of the shape that would develop. Overall, assuming the true shape *is* close to the lead result, then Fig. 15 suggests that the 2-D simulations would tend to underpredict the ratio of surface area to volume as the shape develops, especially in the low reduction cases. As a result, they can be expected to underestimate the true rate of cooling towards the latter stages of the processes, and - in the absence of other factors - might overestimate the temperature in the ring.

Fig. 15 also compares the 2-D model to the 3-D simulation that was set up to explore the plastic collapse limit. Here the difference in height and radial thickness are −8 % and −18 % respectively between 2-D and 3-D simulations, suggesting the 3-D model behaves more similarly to the experiments on these metrics. Some features such as increased axial spread nearest the forming roll (right) and mandrel (left) and underfilling in the flange are also better captured by the 3-D modelling, although it suffers from difficulties with modelling the way the forming roll 'cuts into' the ring.

The aim of the 2-D axisymmetric modelling is to establish an estimate for the likely number of reheats required in processing Inconel 718, a high value engineering material. The comparison on plain rolling shows the 2-D model captures the cooling behaviour very well and provide accuracy within 1–2 %. This accuracy is likely to drop at higher reduction rates where dissipation is a bigger factor since the 2-D model does not capture important shear strains, underestimating the plastic heating. Volume losses due to ALE and the inaccuracies in modelling the

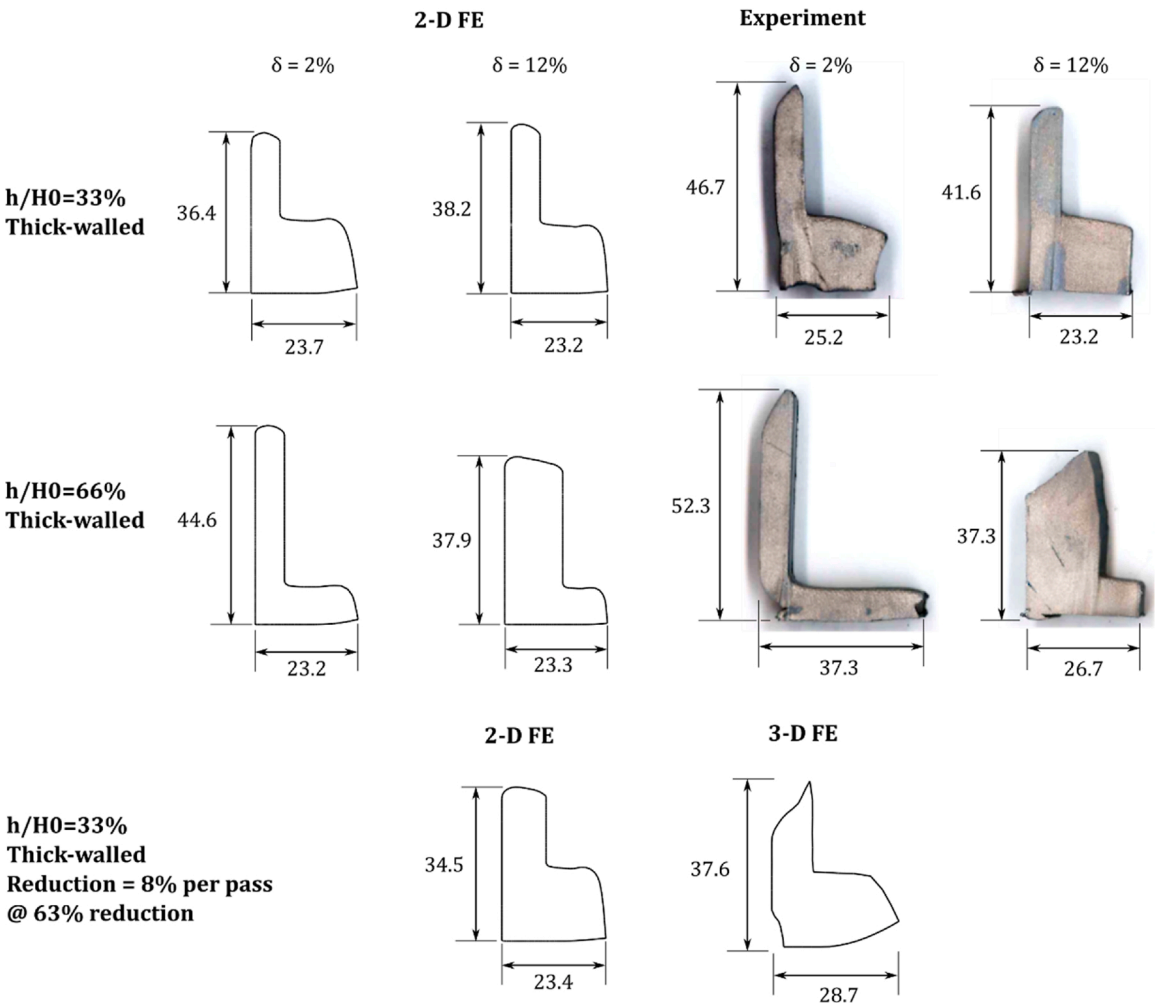

Fig. 15. Profile rolling: 2-D axisymmetric FEM of Inconel 718 vs experimental rolling of lead and 3-D FEM simulation of Inconel 718.

shape as it develops conversely suggest that in some cases the cooling rate may be underestimated towards the later stage of the process. However, the reheat modelling only requires coarse accuracy – given the nature of the criterion imposed - and so the predictions, trends and conclusions drawn from the 2-D modelling are expected to be of value.

4.3. Overall 'design of experiments and FE'

A total of 22 experiments, 22 simplified 2-D FEA simulations and two 3-D FEA simulations were carried out to explore the operating window of the novel L-shape process, as detailed in Table 4. Two of the three main variables explored relate to the target product - the profile height, γ, and the slenderness, λ, as introduced in Eqs. 5 & 6. The third, the reduction, δ, is a variable that a machine operator could vary. The aim is to establish the limiting profile depth, ψ in each case (Eq. 4).

Table 4
Design of experiments and FE in this study. Asterisk denotes the experiment that underwent damage investigation. Double asterisk denotes 3-D FEA performed.

Slenderness ($\lambda = T_0/IR_0$)	Initial profile height ($\gamma = h_0/H_0$)	Reduction in thickness per revolution (δ)	Targeted total reduction in wall thickness (ψ)
3	0.33	2 %, 4 %, 8 %**,12 %	75 %
3	0.67	2%*, 4%*, 8%, 12 %	75 %
6	0.33	2 %, 4 %, 8 %, 12 %	75 %
6	0.66	2 %, 4 %, 8 %, 12 %	75 %
10	0.33	2 %, 4 %, 8 %**	75 %
10	0.66	2 %, 4 %, 8 %,	75 %

The three ring slenderness values cover the range from 3 to 10, almost the entire range previously studied as shown in Table 1 above, but this is the first study to cover more than one slenderness. The slenderness of 3 is a thicker-walled ring than previously thought to be achievable by 'conventional' profile rolling (Cleaver et al., 2017), whereas 10 is relatively thin-walled and it is likely that a plastic collapse will occur early in the process. The two values of the initial profile height were chosen, 33 % and 66 %. As detailed in Table 1, almost all previous work created *final* profile heights of 50 % or less; this study goes well beyond this. This is significant because the larger the profile height the larger the possible material and cost saving.

For each set of parameters describing a target product – i.e. each row in Table 4 - four different reductions in thickness per pass, δ, were used. The range is representative of typical industrial practice. There is a strong focus on reduction because a plant operator may have an opportunity to optimize this; too high and it seems more likely that collapse will occur, too low and the process will take longer, leading to more reheats.

Rather than continue until the ring is so thin it would not be useful, a challenging target reduction in wall thickness, ψ, of 0.75 was set. Each trial was stopped at this point, unless otherwise limited.

The 2-D finite element simulations covered all 22 cases. These have process times ranging from 8 to 154 s. By comparison, a typical process time for rolling Inconel 718 is of the order of 45 s (excluding transfer time) before a reheat is needed, suggesting that in some cases several

reheats may be needed to reach completion (Lohmar et al., 2020). Meanwhile, the ultrasonic testing was carried out on the case marked with an asterisk; these were selected as the large profile height means they experience a large amount of deformation in total but may be most vulnerable to damage - the literature suggests that smaller reductions in thickness per pass may induce more damage (Wang et al., 2016).

5. Results: limits to shaping without ring growth

The results of the novel shaping experiments are presented; the ring shape for each of the 22 experiments is shown and a detailed description of how the ring profile develops is given for two contrasting experiments. As expected, a key limit is plastic collapse, and this is analyzed further, whilst the results of the ultrasonic damage evaluation are shown. Finally, the thermal-mechanical FE simulations are provided.

5.1. Experiments: plastic collapse

The full set of results is shown in Figs. 16–18. Out of the 22 trials, 8 could be completed without a full-scale collapse. The influence of slenderness is clear: a reduction in thickness ψ of 75 % was achieved in the majority of thick-walled rings (5 out of 8), whereas it was achieved in far fewer medium-walled rings (2 out of 8) and only one thin-walled ring (1 out of 6).

The profile height has an equally strong influence: many of the trials with profile height $\gamma = 0.33$ reached a 75 % reduction in wall thickness (7 out of 11), whereas far fewer trials with profile height $\gamma = 0.66$ reached the profile depth of 75 % (2 out of 11).

Meanwhile, the reduction in thickness per pass, δ, plays a role too: the smaller the better. The proportion of trials achieving ψ of 75 % reduces with increasing delta for $\delta = 2$ %, 4 % and 8 % it is (4 out of 6), (3 out of 6) and (1 out of 6) respectively.

In each case, the limiting factor is plastic collapse – a feature that is clearly seen in Fig. 16. The influence of the three variables studied is summarized in Fig. 18: one of the key results of this study. Previous trials on profile rolling summarized in Table 1 are also placed on the left plot, though their height profile may differ. These used different methods of constraint, pre-shaping of the blank and so on as described in Section 2. The trials conducted in this paper using the shaping without ring growth method have produced slightly deeper profiles than previously reported, over a broader range of ring slenderness and profile heights.

To give a sense of what happens during the process, a detailed picture of two experiments is now shown, one where plastic collapse occurred and the second where it did not.

The successful trial highlighted had slenderness $\lambda = 6$, initial profile height $\gamma = 33$ %, and reduction in thickness per pass $\delta = 2$ % - see Fig. 19. The trial continued until the target reduction in wall thickness, ψ of 75 % was achieved. The profile scans and video stills show that the radial position of the upper thin-walled region remains constant throughout the experiment, as expected. Both the rolling force and the constraint roll forces quickly increase over the course of the initial revolutions and reach a steady value. The ring grows significantly in height, and, the depth of profile increases steadily as the upper region reduces in thickness, and the lower region retains close to its original thickness. In the early to middle stages the measured height growth is slightly higher than the height growth predicted by the constant volume model described in Section 3.1; this is – at least in part – because the laser measures the peak height, and not the average. The variation in height can be seen in the cross-sections in Fig. 17. Towards the end of the trial, $\psi > 0.65$, there seems to be a change in behavior: the constraint roll forces drop, the rolling force increases, and the profile depth appears to grow at larger rate than expected. This might indicate the onset of a plastic collapse or other failure mode that has not yet fully developed by the point where $\psi = 75$ %.

In comparison, during the trial on a ring with the same slenderness and reduction per pass, but with initial profile height $\gamma = 66$ %, a plastic collapse occurred – see Fig. 20. The experiment was stopped when $\psi = 0.42$. Looking at the force trend, especially the oscillating constraint roll forces, it seems like the plastic collapse starts at some point between $\psi = 0.3-0.4$. By the time ψ reaches 0.42 it becomes impossible to continue the process.

Fig. 17 showed the ring cross-sections. Although these are broadly L-shaped as expected, their form is not flawless. In all cases, the ring grows in height non-uniformly, with greater height growth found on the outer radial surface. The thick lower flange region also does not always remain rectangular, in some cases the new axial surface slopes downwards, or a cavity forms on the inner radial face.

Part of the motivation for this work is material saving, and therefore Fig. 21 presents a metric that takes into account these errors in form: each example cross-section pictured has three perimeters: 1) a red perimeter around the produced cross-section; 2) a black L-shape that is the largest possible L-shape that can be made from the actual product, comprised of two rectangular areas, and 3) a blue rectangle that envelopes the black L-shape representing the size of workpiece needed to create the black L-shape by plain (rectangular cross-section) ring rolling. The material saving quoted is calculated as the difference between the area of the blue rectangle and the shape enclosed by the red outline divided by the area of the blue rectangle.

Fig. 21 shows that for low profile height, and small reductions (2 or 4%), the material saving is close to the level expected in the absence of plastic collapse or form errors. For higher reductions, and in many of the larger profile height cases ($\gamma = 66$ %) the material saving is lower than expected, principally because of early plastic collapse.

The largest potential material saving is 65 % ($\gamma = 66$ %, $\lambda = 3$, $\delta = 2$ %), whilst the saving is consistently around 40–50 % for the low profile height ($\gamma = 33$ %) and small reductions; higher than previously demonstrated in the literature, 45 %, which was achieved using a full external die around the ring. Achieving these savings in practice is of course provisional on avoiding other limiting factors such as ductile damage or thermal processing limits as will be explored in subsections 5.2 and 5.3.

5.1.1. Analysis of plastic collapse

The novel shaping without ring growth approach was shown to produce deep and tall profiles, limited by plastic collapse. This important limit is analysed further here.

The 'back pressure', σ_b generated by the constraint rolls is thought to be important feature of the process both enabling axial material flow, but also contributing to plastic collapse. Fig. 22 shows the evolution of σ_b in each of the trials, compared to the saturation flow stress for lead, $\widetilde{\sigma_f}$ at strain rate 0.1/s, of 26 MPa (Cleaver and Allwood, 2019). The general trend is much as anticipated in Fig. 9a: σ_b builds up over the initial revolutions until it is large enough to prevent circumferential flow. It remains roughly at this level until either the trial ends, or the strength capacity of the ring is exceeded, collapse onset occurs and σ_b oscillates until the trial is stopped.

The pressure to prevent circumferential flow, previously introduced as $\sigma_{b\text{-}ax}$ does not exceed 50 % of $\widetilde{\sigma_f}$. This could be explained by stress superposition. The profile height (γ), ring slenderness and the reduction in thickness per pass (δ) all influence σ_{ax}. For example, for thick-walled rings with $\gamma = 66$ %, σ_{ax} increases from 32 % to 44 % of the flow stress as the reduction increases from 2 % to 8 %. With smaller profile height of 33 % the back pressure is reduced from 32 % to about 17 % of the flow stress: perhaps because the constraint provided by the undeformed flange region is larger.

Our expectation is that for collapse, σ_b should cross a threshold $\sigma_{b\text{-}col}$ whose upper bound is given by the plastic hinge model in 3.11, and Eq. 8. The threshold depends on the ratio of the plastic moment, M_p to the ring radius R. M_p was calculated using the saturation flow stress $\widetilde{\sigma_f}$ (26 MPa) and that the ring shape evolves as described in Section 3.1

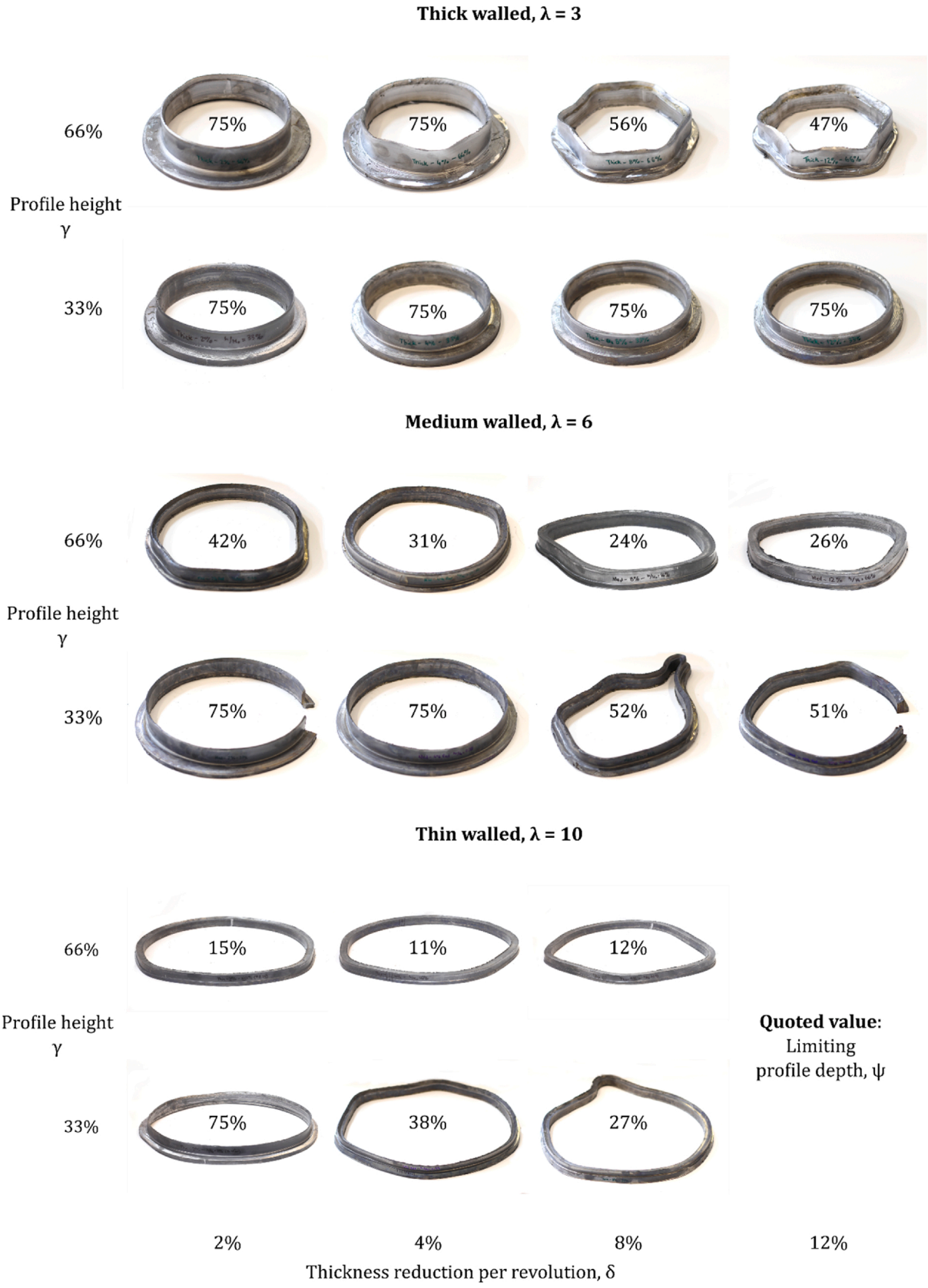

Fig. 16. Limiting profile depth due to plastic collapse: L-shaping without ring growth.

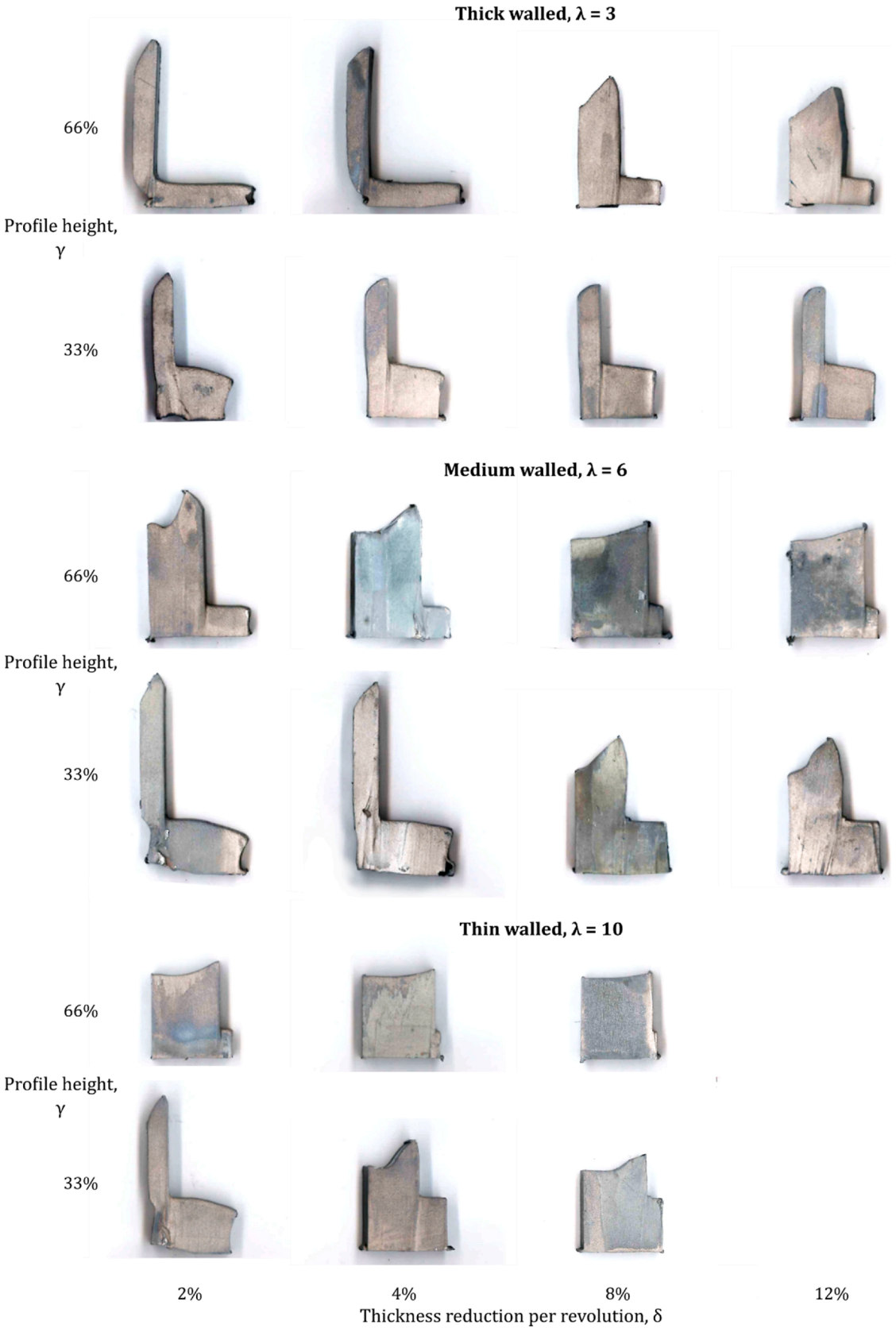

Fig. 17. Cross-sectional profile of rings: L-shaping without ring growth.

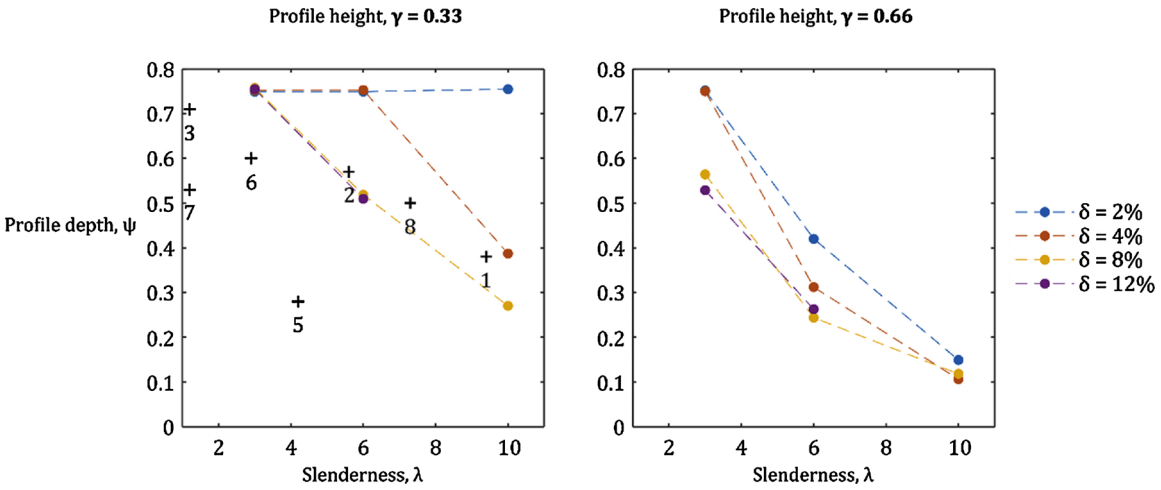

Fig. 18. Summary of the influence of slenderness, λ, profile height, γ, and reduction per pass, δ, on the limiting profile depth ψ due to plastic collapse. Marked points are from previous studies on profile ring rolling, the number refers to the row in Table 1, though their profile height may differ.

Whilst the upper bound threshold is not approached, an empirical scaling of this threshold line – to be introduced shortly - *does* provide a good indication of when collapse will occur, across all trials. This collapse stress reduces through the early stages of the experiment, because Z_p, the plastic section modulus, reduces, whilst R remains largely unchanged. Notably, this drop-off is much less marked than if the ring were to grow in diameter throughout the process since both Z_p would decrease by a greater amount, and R would increase.

The lower bound is developed empirically in Fig. 23. This shows the force generated at constraint roll 4 when collapse occurs plotted against the value of M_p/R at this point in the trial. Collapse is determined by the point where the back pressure begins to oscillate in Fig. 19. For trials that did not result in collapse, the point of peak force is shown. The trials that lead to plastic collapse are red, and those that did not are green. Constraint roll 4 was chosen because it experiences the greatest force – see Figs. 19 and 20 - and has the largest angular spacing between rolls, 60°. The collapse is likely to develop here first.

The upper bound model predicts that all the 'collapsed' trials should lie either on or below the line defined by $F = 15M_p/R$. Whilst this is supported by the data, the upper bound line is much higher than the actual collapse. It is remarkable that a 'lower bound' straight line can be drawn to divide between success and failure. This has a significantly reduced slope, $F = 4.6M_p/R$.

Ideally the lower and upper bounds would be much closer: there are several possible reasons for the divergence: 1) the 'collapse' could occur when the moment is smaller than Mp, 2) the 'force' readings derived from the motor currents may not be accurate, 3) the flow stress may be less than the saturation flow stress, potentially due to either lower hardening or static recrystallisation outside the roll gap or 4) curvature changes in the radial roll bite might play an important role in the collapse, requiring significantly lower constraint roll forces to occur (Cleaver and Allwood, 2019).

It is yet to be established what level of constraint roll force is necessary to prevent ring growth, i.e. the value of the force plateau seen in Fig. 19. If this is known, then it could be combined with the preceding analysis to predict plastic collapse a priori. What is certainly clear from these trials is that six constraining rolls around the ring are sufficient to allow shaping without ring growth *without* plastic collapse in many cases. The larger the reduction, the thinner-walled the ring, and the taller the profile, the more likely it is for plastic collapse to occur.

5.1.2. Comparison of collapse in Inconel 718 to lead

Two 3-D FEM simulations were carried out to indicate how far the plastic collapse results in lead are transferrable to the high value engineering material, Inconel 718. The results are compared in Fig. 24. The first is a thick-walled ring with reduction 8 % where no collapse was seen in the lead experiment; no collapse was seen in the Inconel 718 FE simulation either. The second is a much thinner walled ring, and in this case both the experiment and FE simulation show a collapse.

Fig. 24 also shows the evolution of back pressure σ_b for experiment and simulation normalized by its respective maximum value. The final collapse point – where the process can no longer proceed - in the Inconel 718 simulation occurs at a slightly later point, ψ of about 0.42, compared to 0.27 for the experiment. This may be because the simulation underestimates the radial width of the 'flange', thus underestimating its plastic section modulus. Equally it may be a genuine effect of processing at high temperature: whilst the back pressure for axial flow probably depends on the *average* flow stress, the collapse in bending depends more strongly on the flow stress at the inner and outer radial *surfaces* which are cooler and thus stronger, increasing the hot ring's capacity to avoid plastic collapse.

Overall, these two simulations suggest that the clear *trends* seen in the lead experiments are transferrable Inconel 718, and almost certainly other high value engineering materials.

5.2. Experiments: ductile damage

Previous profile rolling processes are vulnerable to cracking in any under deformed regions of the ring that are 'stretched' as the ring grows. The following presents a study into how far the same problem is found in the novel set-up proposed here with highly restricted circumferential ring growth.

Scanning acoustic microscopy results of the as-cast and pre-rolled lead samples (λ = 3) are shown in Fig. 25. Voids and defects are identified as dots in the scanned images. Any defect larger than 15 microns in the specimens was captured and displayed as a pixel in this analysis. A comparison between the results of the as-cast and the pre-rolled cases (Fig. 25a & b) reveals that a significant number of cavities are present in the as-cast ring were closed during pre-rolling.

Scanning acoustic microscopy results of the two shaped rings indicated in Table 4 are presented in Fig. 26. These are thick-walled parts (λ = 3) with large profile height (γ = 66 %), rolled with reductions in thicknesses δ = 2% and 4%. The results confirm that the number of voids detectable remain much the same as for the pre-rolled case, and certainly do not increase significantly. Whilst this is to be expected in the thin-walled region, which is compressed by the tools, the observation that the flange region is also free of detectable voids is encouraging. This may in part be due the fact that it does not stretch circumferentially.

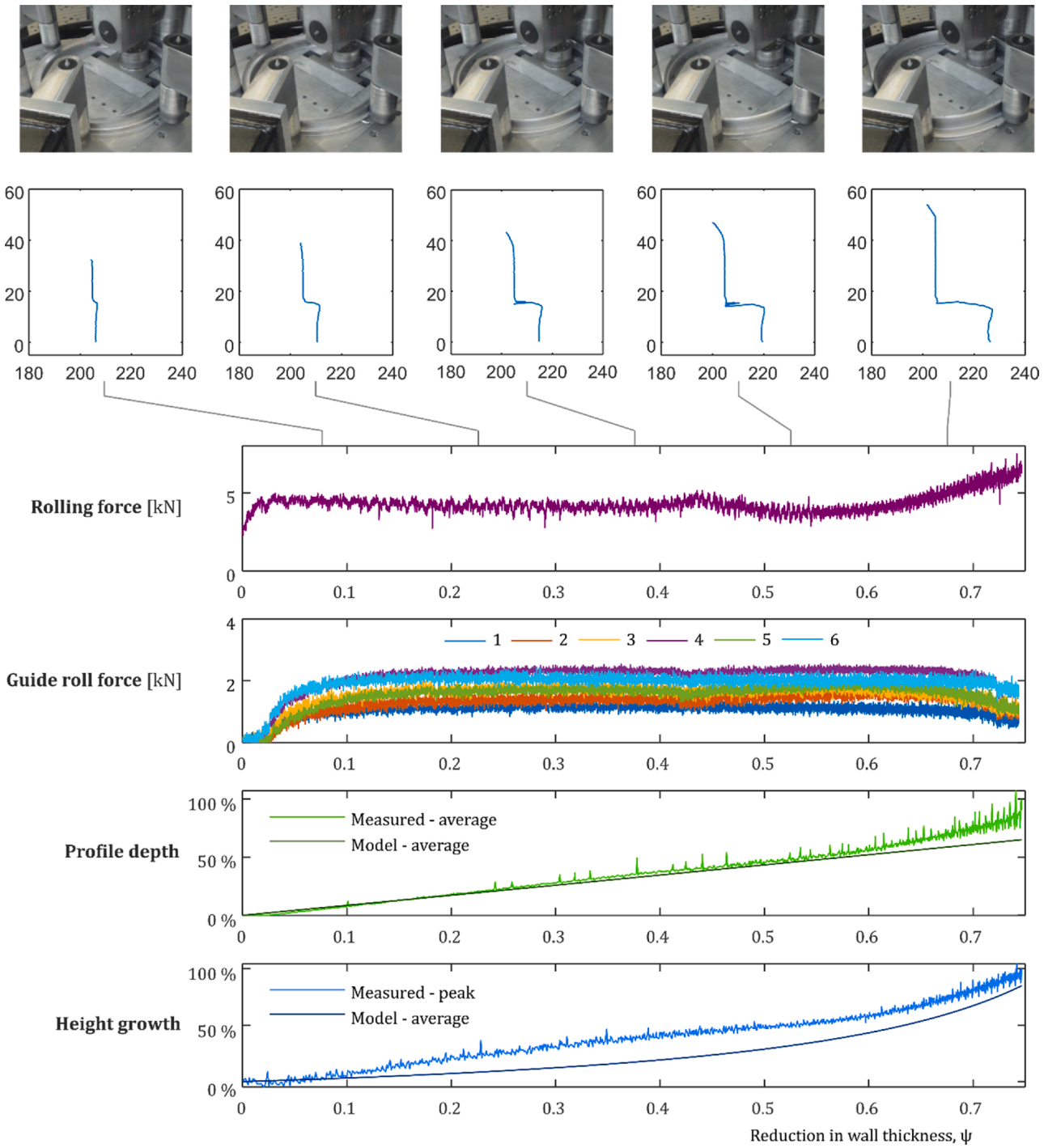

Fig. 19. Successful trial: evolution of ring shape and rolling forces for a 'successful' shaping without ring growth trial, $\lambda = 6$, $\gamma = 33$ %, and $\delta = 2$ %.

5.3. *FE Simulations: thermal processing limit*

Results of the simplified 2-D axisymmetric Finite Element modelling are presented. These were set up to estimate the reheat requirements of applying the shaping without ring growth method to Inconel 718, as an example of a high value engineering material.

Fig. 27 illustrates a series of temperature profiles at selected points through an exemplar simulation, $\lambda = 3$, $\gamma = 33$ %, $\delta = 8$ %, to highlight the reheat modelling process. The process was completed in 16 revolutions, and required one reheat.

To begin, in subfigure a, the ring loses an average 57 °C during the 15 s transfer to the machine, cooling from furnace temperature of 1030 °C to 973 °C. Subfigure b then shows the ring at the end of the 11th revolution prior to passing through the roll gap for the 12th time. At this point the average temperature has reduced by a further 23 °C, but the reheat criterion has not yet been triggered. During forming there is both cooling due to conduction and heating due to plastic dissipation. On average the temperature drops by a further 2 °C - subfigure c right after rolling pass 12. By the end of the subsequent cooling stage in subfigure d, the temperature has dropped to 948 °C on average, and the reheat criterion *is* triggered at the end of this 12th revolution. The subsequent temperature distribution after reheating and transferring to the machine is then shown in subfigure e. The average temperature is restored to 960 °C, with no cold edges. It was possible to complete the process after the

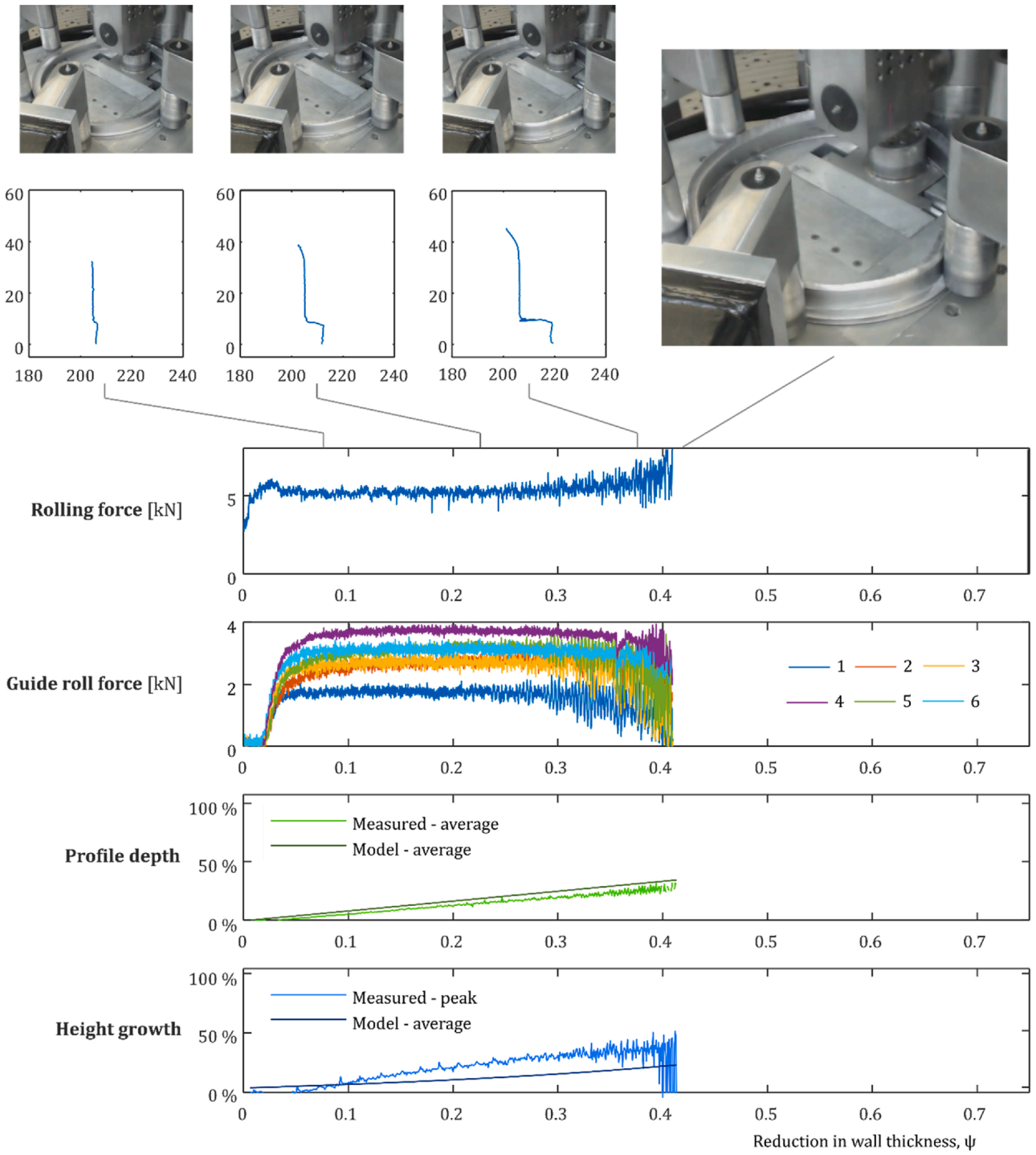

Fig. 20. Plastic collapse: evolution of ring shape and rolling forces for a shaping without ring growth trial where plastic collapse occurred, $\lambda = 6$, $\gamma = 66$ %, and $\delta = 2$ %.

16th revolution without requiring another reheat; the final temperature distribution in shown in subfigure f. The corresponding equivalent plastic strain distributions for the subfigures a – f are given below the temperature plots for reference.

The same method was applied to all 22 simulations to estimate the achievable profile-depth if no more than two reheats are allowed. In half of the cases it was possible to achieve the targeted profile depth of 0.75 with two or fewer reheats – see Fig. 28. The number of reheats is strongly influenced by the reduction per revolution, as expected. The largest profile achievable in two reheats with 2 % per revolution was just 0.52, whereas all the simulations with 12 % per revolution achieved 0.75. The slenderness and profile height also have an influence: thicker walled rings do not cool as rapidly, and so greater profile depths were achieved, for example with a reduction of 4 % the achievable profile depth was 0.75 for thick walled compared to 0.46 for the thin-walled ring.

These findings are of course predictions only and subject to errors introduced by the modelling assumptions, especially the 2-D approach used. For instance, Section 4.23 indicated that the simulations for $\delta > 2$ % might significantly underestimate the impact of

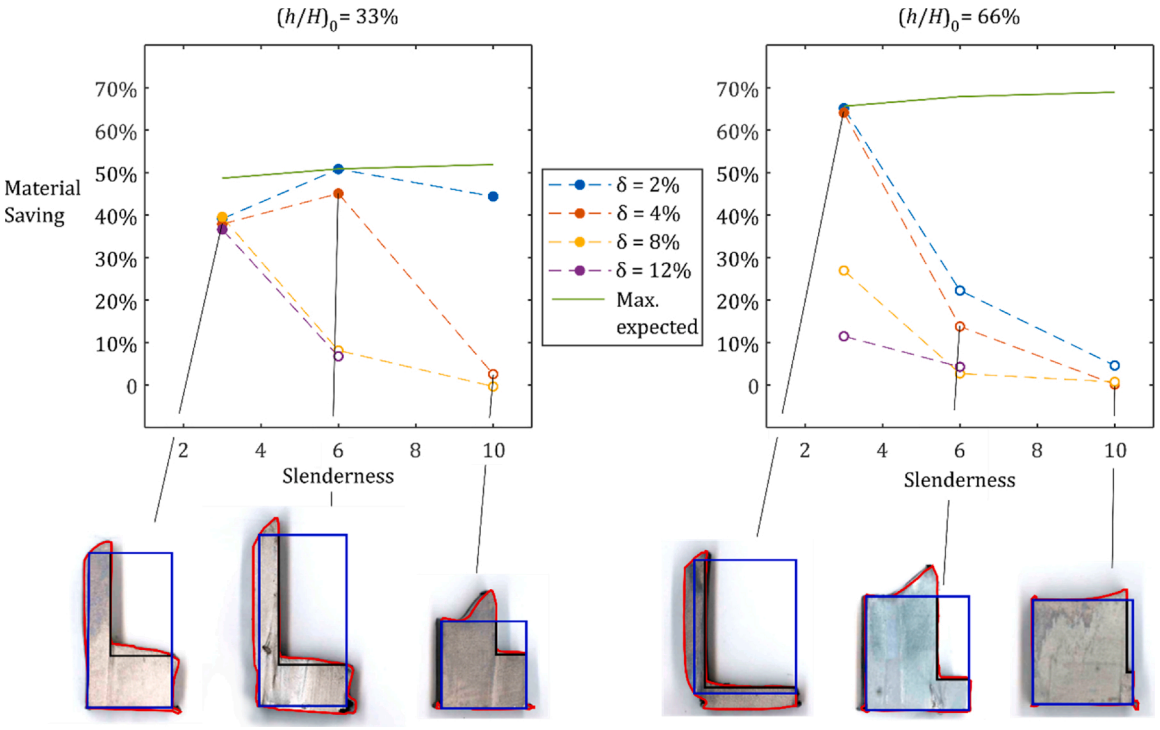

Fig. 21. Estimate for the material saving by shaping without ring growth, actual vs 'ideal'. Hollow circles mark trials were there was an early onset of plastic collapse.

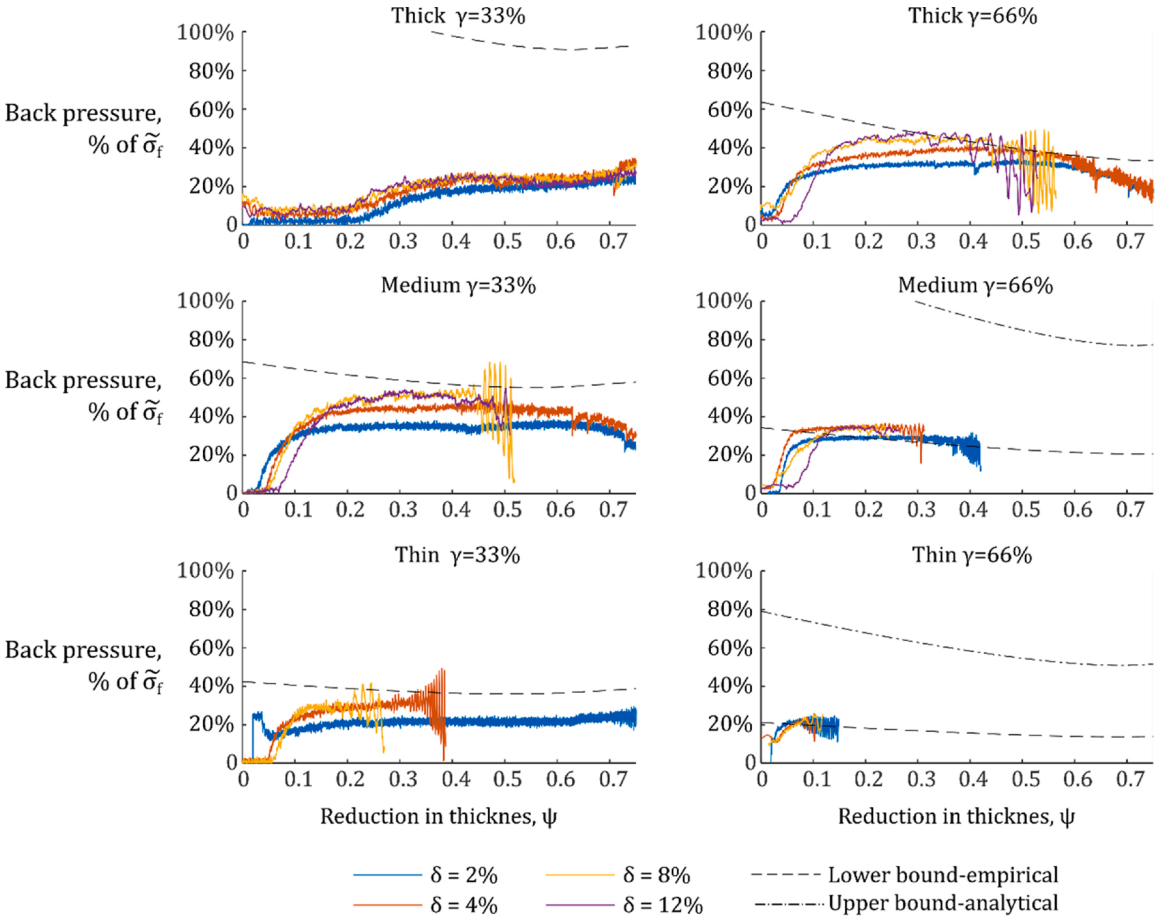

Fig. 22. Evolution of the back pressure vs an upper and lower bound for collapse.

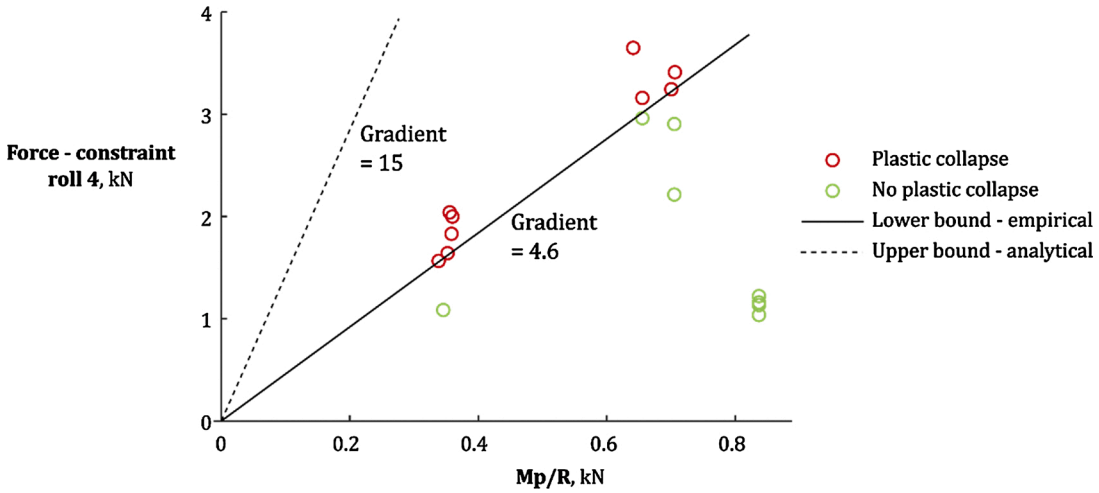

Fig. 23. Correlation between constraint roll 4 force and M_p /R at onset of collapse (red), or peak force (green) (For interpretation of the references to colour in this figure legend, the reader is referred to the web version of this article).

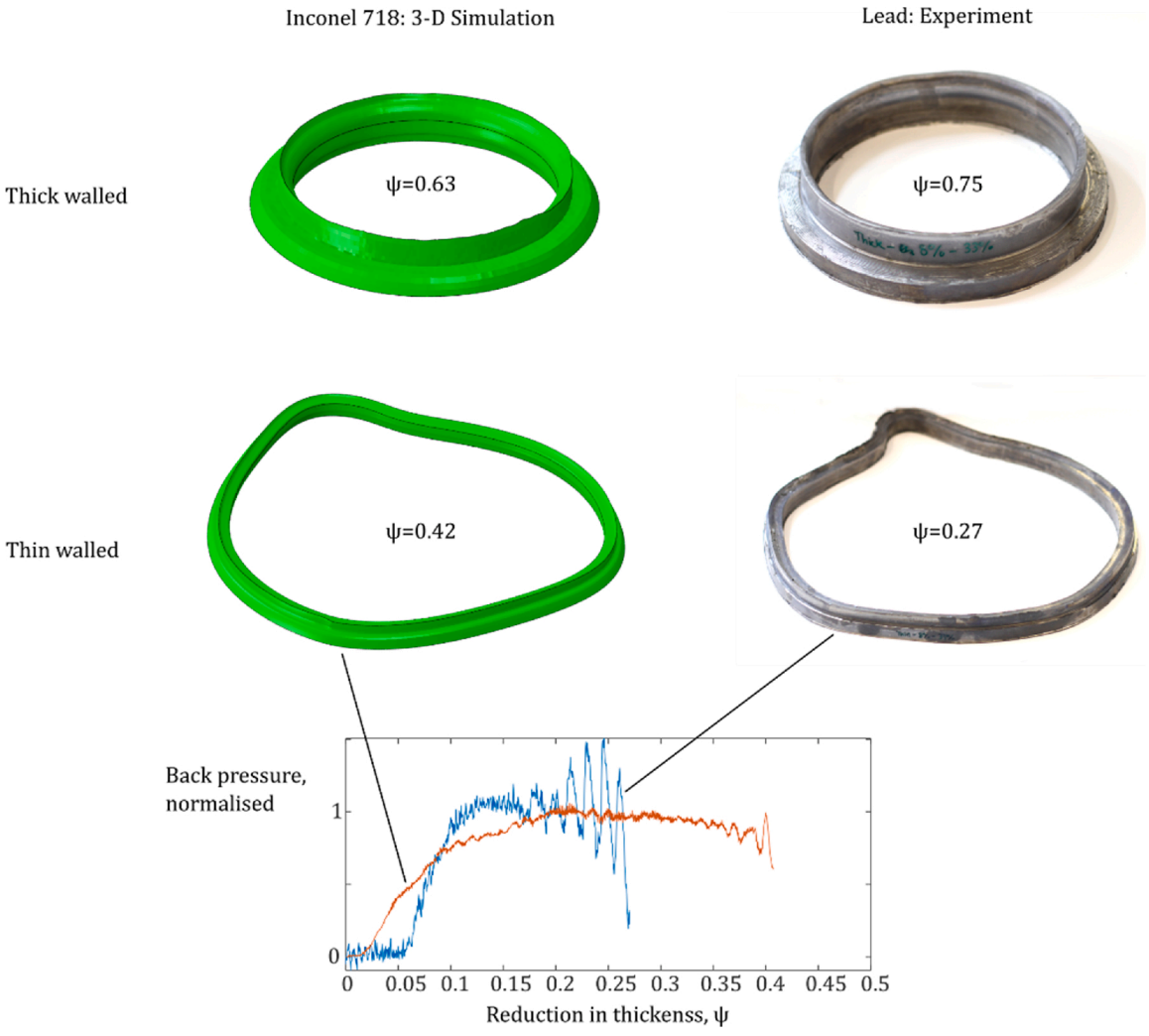

Fig. 24. Comparison of plastic collapse in 3-D simulation of Inconel 718 and corresponding lead experiments.

plastic dissipation. Here, the process might be possible with fewer reheats. This is only really of significance to the 4 % reduction cases since all the 8 % and 12 % reduction simulations completed in two or fewer reheats anyway.

6. Discussion

The novel ring shaping process has been evaluated for a range of ring sizes, profile heights and thickness reduction rates, through experiments

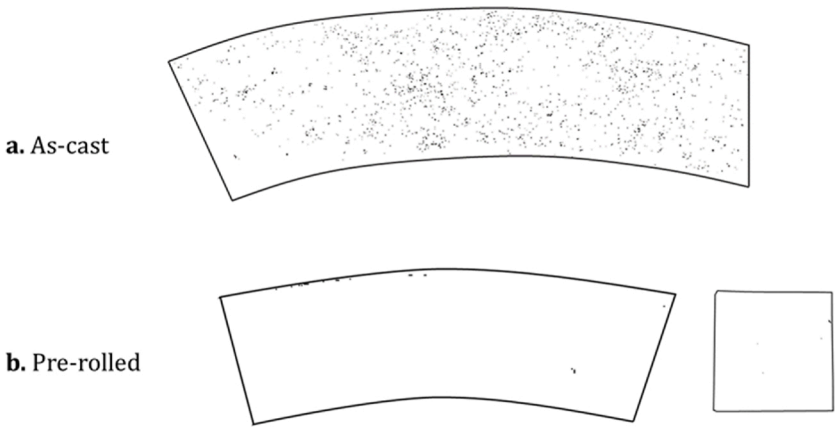

Fig. 25. SAM images of voids > 15 μm for **a.** as-cast lead preform – horizontal section **b.** pre-rolled ring (λ = 3) – vertical and horizontal section.

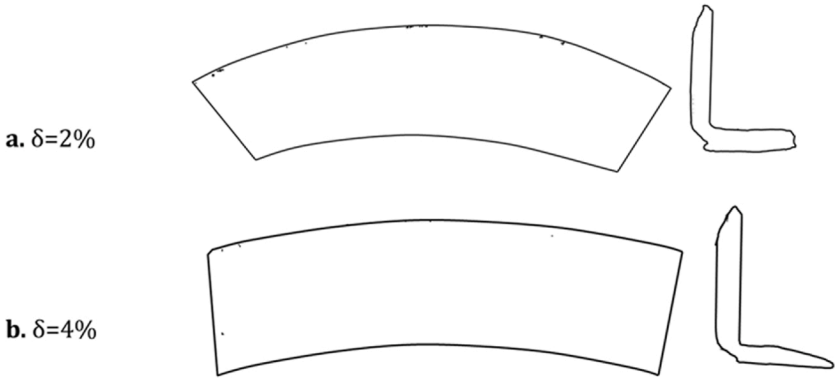

Fig. 26. Shaped rings: SAM images of voids > 15 μm for horizontal and vertical sections of the ring for thick-walled rings (λ = 3) with large profile height (γ = 66 %) **a.** δ = 2 % and **b.** δ = 4 %.

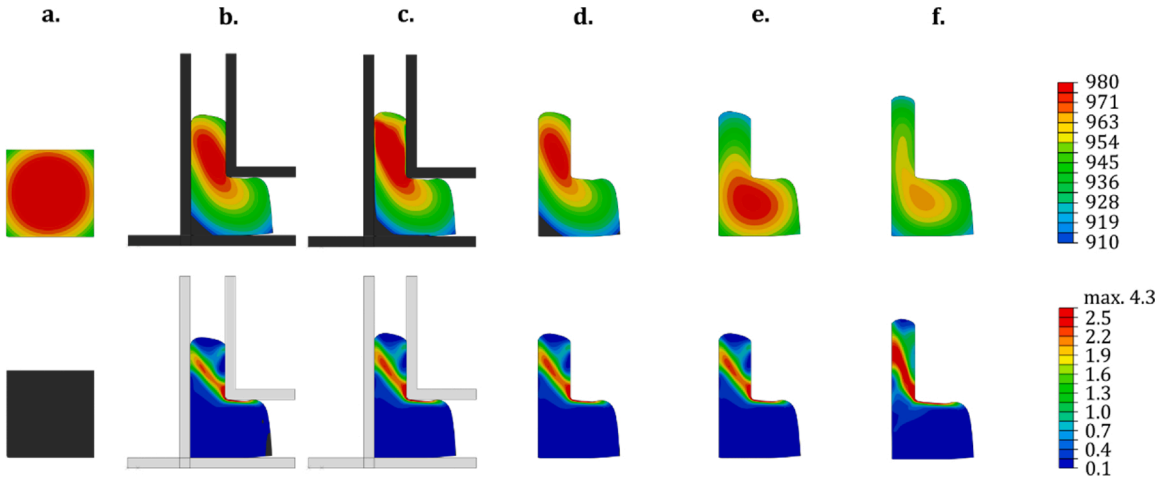

Fig. 27. Temperature and equivalent plastic strain profiles predicted FE at selected points through a single trial λ = 3, γ = 33 %, δ = 8 % **a.** start of rolling, after transfer **b.** end of 11th revolution **c.** after 12th forming pass **d.** end of 12th revolution **e.** after first reheat and transfer **f.** end of process, 16 revolutions.

on lead and 2-D and 3-D simulations of a high value engineering material, Inconel 718. The experiments showed profiles deeper than or comparable to previous studies were achieved by using six constraint rolls around the ring to prevent circumferential ring growth, without requiring a large die around the ring or a shaped ring preform. A key objective of the study was to explore the process operating window, and various limiting factors were considered including damage accumulation, shaping accuracy, plastic collapse of the ring and excessive cooling. The latter two emerged as the most prominent, and these are brought together in Fig. 29, indicating a series of operating window plots for hot processing of a high value engineering material, Inconel 718.

Fig. 29 shows operating windows for differing ring slenderness (up and down) and profile height (left and right). The limit of excess ring cooling was considered with a reheat triggered if the temperature falls below 910 °C and the limit of no more than two reheats is plotted on Fig. 29 in red. Plastic collapse was studied experimentally through trials

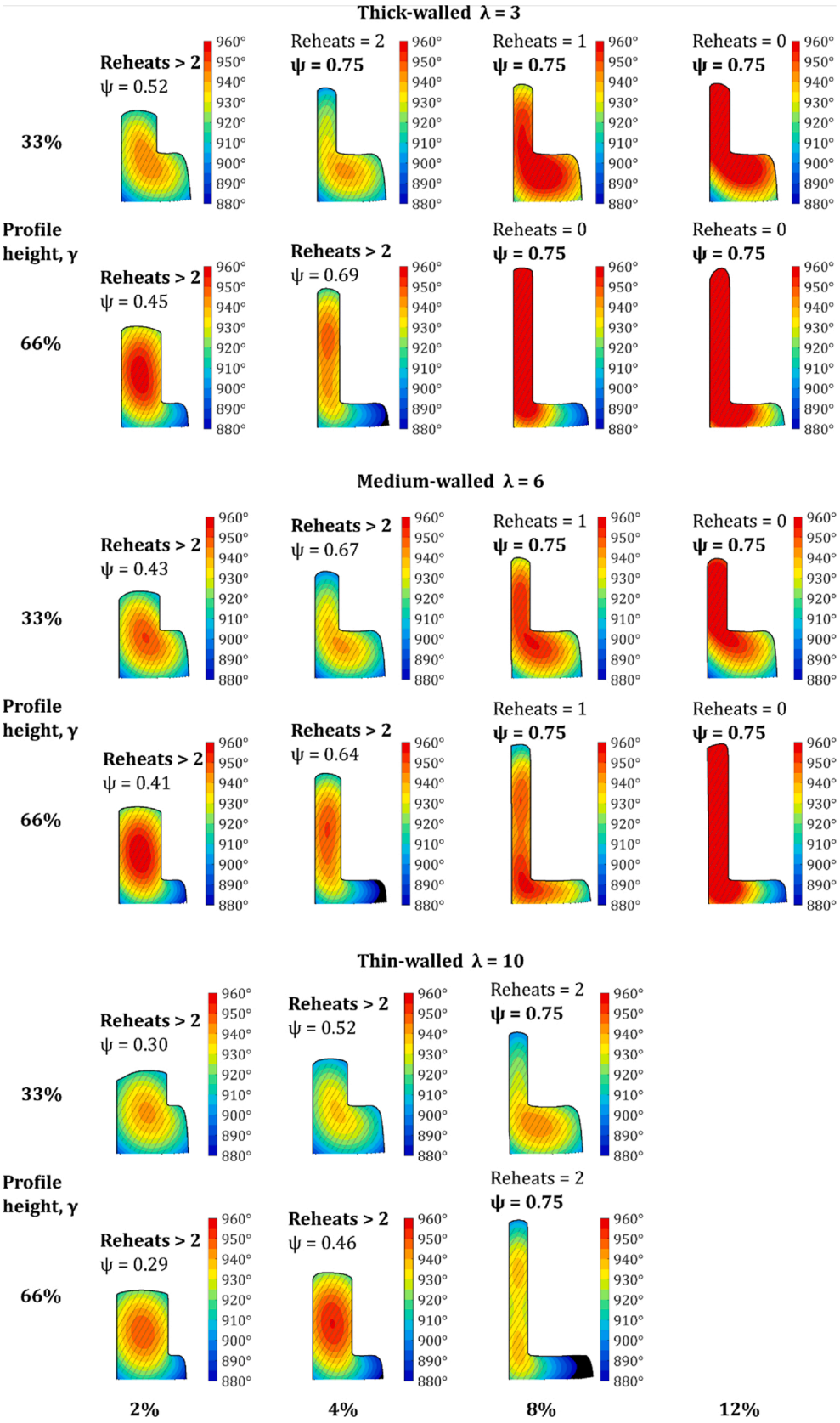

Fig. 28. Achievable profile depth for L-Shaping in Inconel 718 in two or fewer reheats.

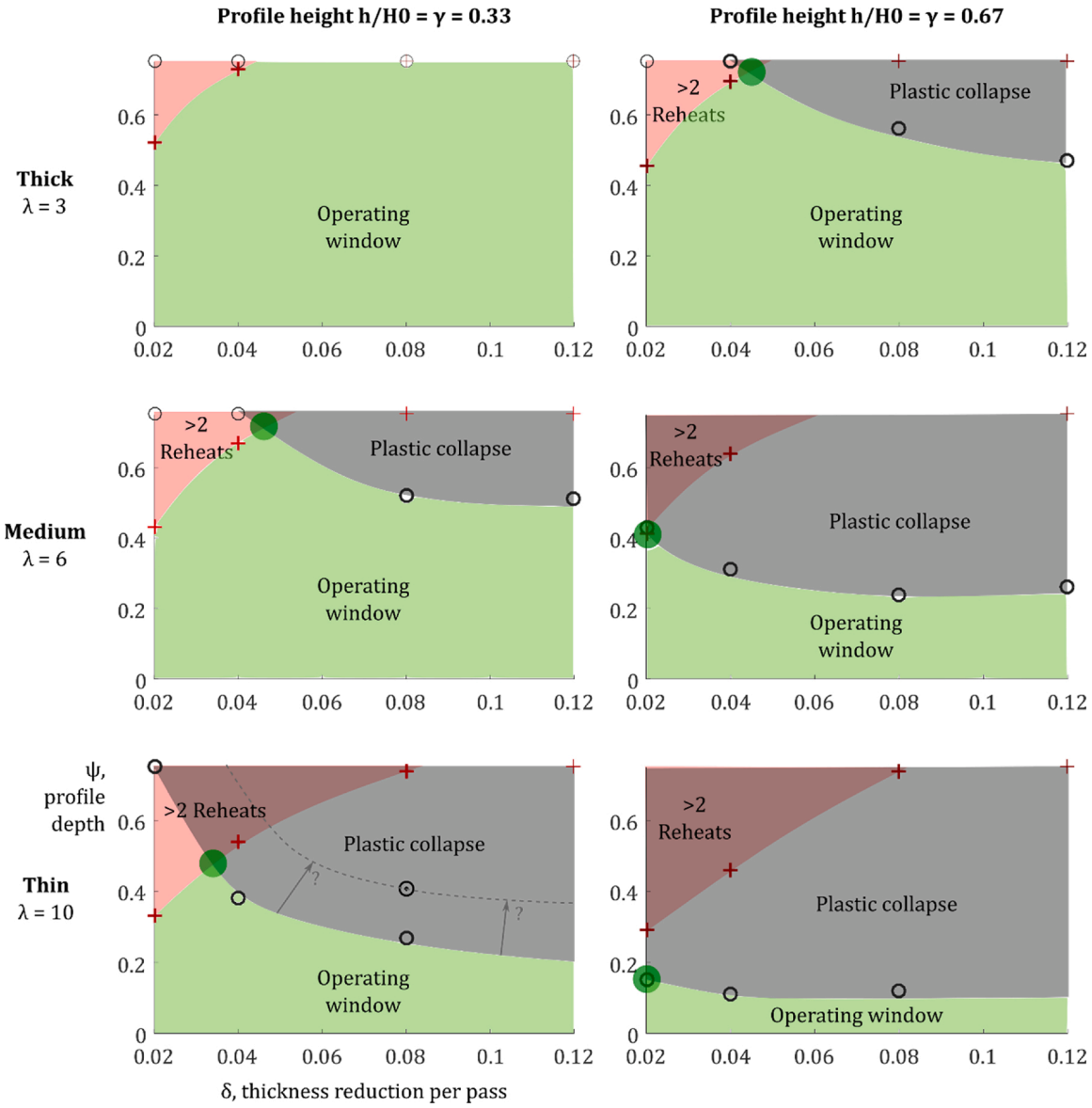

Fig. 29. Combination of limits to shaping without ring growth for Inconel 718 as an example high value engineering material. Green circle marks optimum operating point. Black double circle marks result of 3-D FEM simulation on Inconel 718 (For interpretation of the references to colour in this figure legend, the reader is referred to the web version of this article).

on lead - a model material that is in hot forming condition already at room temperature. As previously discussed, these observations are broadly transferrable to any high value metallic material since the driving force for collapse - the force exerted by constraining guide rolls - and the ring's ability to withstand it are equally linked to the flow stress. The region where plastic collapse is expected is therefore marked in grey. As discussed in 5.12 the 3-D FE simulation result for Inconel 718 – marked with a double circle on Fig. 25 – suggests that the grey region may be somewhat conservative for this material.

The subfigures show a trade-off between low reduction in thickness per pass which avoids plastic collapse, and higher reductions that avoid excessive cooling. This is particularly important for thin-walled rings with smaller profile height ($\lambda = 10$, $\gamma = 33$ % - bottom left of Fig. 25). Here, whilst a profile depth of 75 % was achievable without collapse in the experiments, the low reduction required violates limit of two reheats, and therefore a profile depth of only about 45 % appears possible; if the reduction in thickness was around 3.5 % per revolution. For larger profile height ($\gamma = 66$ %) plastic collapse is the single limiting factor, except in the thick-walled case (top right) where a limit of two reheats reduces the achievable profile depth to slightly below 75 %.

Along with profile depth, the thermal processing limit has a modest knock-on impact on material saving potential. For instance, the maximum material saving of 65 % found in the experiments on lead (for $\lambda = 3$, $\gamma = 66$ %) is ruled out by the low reduction in thickness per revolution used, $\delta = 2$ %. Fig. 29 suggests that avoiding more than 2 reheats reduces this saving to around 60 %. The biggest impact would – again - be on rings with $\lambda = 10$, $\gamma = 33$ % where avoiding more than 2 reheats could reduce material saving from 45 % to around 30 %. Overall, however, it seems that the material saving potential in Inconel 718 is only weakly affected by thermal processing limits.

In previous work on profiled lead and aluminium rings cracking was found in under-deformed regions of the expanding ring. However, in the shaping without ring growth process the under-deformed flange is not stretched significantly - the ring is not growing - and none of the rings showed visible signs of cracking. An analysis of voids in the flange region found no evidence of void formation during the process, and so for lead at room temperature cracking does not appear to be a limiting factor. Unlike plastic collapse this finding may *not* be transferrable to other

materials and require further verification since damage is strongly influenced by both material properties and processing temperature. As well as void formation, the difference in plastic strain between regions of the workpiece might also influence the grain size/morphology, which could in turn influence the service performance. This is yet to be investigated.

Whilst there is still some uncertainty, this study *does* suggest that operating conditions can be found where shaping without ring growth is feasible for high value engineering materials, even in Inconel 718, a challenging material to process. If thinner-walled rings are required, then the plastic collapse limit could be improved by using a larger number of constraining rolls around the ring.

7. Conclusions

The study has found that:

1 Six constraint rolls can be used to prevent ring growth in ring rolling, generating sufficient back pressure to enable ring shaping by axial material flow.
2 Profiles of depth 75 % of the original wall thickness are achievable, saving up to 60 % of the material over non-shaped rolling if an L-shape cross-section is needed.
3 The shaping without ring growth' process is limited by two main factors: plastic collapse and – depending on the material used - excessive ring cooling.
4 Plastic collapse occurs when the constraint roll force exceeds the capacity of the ring to withstand this force.
5 Thicker-walled rings are much less prone to collapse (2 out of 8 studied collapsed before a profile-depth of 75 % was achieved) than medium walled (6 out of 8) and thin-walled (5 out of 6).
6 Axisymmetric thermally coupled modelling can be used to indicate cooling during hot rolling, finding that for Inconel 718 multiple reheats would be required in most cases (17 out of 22).
7 The numbers of reheats increased significantly as the reduction in thickness per pass decreases, whereas the possibility of plastic collapse reduces. Reductions per pass in the order of 3–4 % were found to be optimal in most cases.

CRediT authorship contribution statement

Christopher John Cleaver: Conceptualization, Methodology, Software, Validation, Formal analysis, Data curation, Investigation, Writing - original draft, Writing - review & editing, Visualization. **Johannes Lohmar:** Conceptualization, Methodology, Software, Formal analysis, Writing - review & editing, Visualization. **Saeed Tamimi:** Investigation, Visualization.

Declaration of Competing Interest

The authors report no declarations of interest.

Acknowledgements

Dr. Cleaver's work on this study was funded by the UK Engineering and Physical Sciences Research Council (EPSRC), under grants EP/S019111/1 and EP/N02351X/1. Dr. Tamimi would like to thank the Advanced Forming Research Centre (AFRC) for the support with the study. The authors are immensely grateful for the advice provided by Prof. J.M. Allwood throughout the period of this study.

References

Allwood, J., Kopp, R., Michl, D., Music, O., Öztop, M., Stanistreet, T.F., Tekkaya, A.E., Tiedemann, I., 2005. The technical and commercial potential of an incremental ring rolling process. CIRP Ann. Manuf. Technol. 54 (1), 233–236.
Cleaver, C.J., 2017. The development of an incremental ring rolling process with axial and circumferential constraints. PhD thesis, University of Cambridge.
Cleaver, C., Allwood, J., 2017a. Incremental profile ring rolling with axial and circumferential constraints. CIRP Ann. Manuf. Technol. 66 (1), 285–288.
Cleaver, C.J., Allwood, J.M., 2017b. Incremental ring rolling to create conical profile rings. Proceedia Engineering 207, 1248–1253.
Cleaver, C.J., Allwood, J.M., 2019. Curvature development in ring rolling. J. Mater. Process. Technol. 267, 316–337.
De Souza, U., Vaze, S., Pursell, Z., Phillips, K., 2003. Profile ring rolling. Adv. Mater. Process. May 2003.
Euroforge, 2020. 2017-2018 Production Figures – World-wide. Web Resource. https://www.euroforge.org/statistics/production-figures.html.
Forging Industry Association, 2015. 2014 Annual Forging Sales. Web resource: https://www.forging.org/about/fia-press-releases.
Garrison Jr., W.M., Moody, N.R., 1987. Ductile fracture. J. Phys. Chem. Solids 48 (No. 11), 1035–1074.
Han, X., Hua, L., Zhou, G., Lu, B., Wang, X., 2014. FE simulation and experimental research on cylindrical ring rolling. J. Mater. Process. Technol. 214, 1245–1258.
Hawkyard, J.B., Moussa, G., 1984. Studies of profile development and roll force in profile ring rolling. Proceedings of the 3rd International Conference on Rotary Metalwork Processes 301–310.
Kluge, A., Breit, T., Wiegels, H., Kopp, R., 1997. Radial-Gesenkringwalzen Von Ringen mit umlaufenden profilen. Stahl und Eisen 117 (8), 63–66.
Koppers, U., Kopp, R., 1992. Geometrie der Umformzonen beim Ringwalzen. Steel Res. 63 (2), 74–77.
Lohmar, J., Cleaver, C.J., Allwood, J.M., 2020. The influence of constraint rolls on temperature evolution and distribution in radial ring rolling. J. Mater. Process. Technol. 282, 116663.
Lu, B., Wang, L., Geng, Z., Huang, Y., 2017. Heat transfer characteristics of Billet/Die interface and measures to relieve thermal stress for hot forging die. Int. J. Thermophys. 38 (7).
Marczinski, H.J., 1984. The Hot ring rolling process and its integration into automatic production lines. Proceedings of the 3rd International Conference on Rotary Metalwork Processes 251–265.
Medeiros, S.C., Prasad, Y.V.R.K., Frazier, W.G., Srinivasan, R., 2000. Microstructural modeling of metadynamic recrystallization in hot working of IN 718 superalloy. Mater. Sci. Eng. A 293 (1–2), 198–207.
Moussa, G., 1981. Investigations in the Rolling of Profiled Rings. PhD Thesis. University of Manchester Institute of Science and Technology.
Oh, I.Y., Hwang, T.W., Woo, Y.Y., Yun, H.J., Moon, Y.H., 2019. Process-induced defects in an L-shape profile ring rolling process. Int. J. Mater. Form. 12, 727–740.
Qian, D.-S., Hua, L., 2010. Blank design optimization for stepped-section profile ring rolling. Sci. China Ser. E Technol. Sci. 53, 1612–1619.
Qian, D.-S., Zhang, Z., Hua, L., 2013. An advanced manufacturing method for thick-wall and deep-groove ring-combined ring rolling. J. Mater. Process. Technol. 213, 1258–1267.
Salimi, M., 1988. An Investigation into the Rolling of Thick and Thin Walled Profile Rings. PhD Thesis. Victoria University of Manchester.
Seuren, S., Seitz, J., Krämer, A., Bambach, M., Hirt, G., 2014. Accounting for shear deformation in fast models for plate rolling. Prod. Eng. Res. Devel. 8, 17–24.
Thomas, A., El-Wahabi, M., Cabrera, J.M., Prado, J.M., 2006. High temperature deformation of Inconel 718. J. Mater. Process. Technol. 177 (1–3), 469–472. https://doi.org/10.1016/j.jmatprotec.2006.04.072.
Tiedemann, I., Hirt, G., Kopp, R., Michl, D., Khanjari, N., 2007. Material flow determination for radial flexible profile ring rolling. Prod. Eng. 1 (3), 227–232.
Wang, C., Geijselaers, H.J.M., Omerspahic, E., Recina, V., van den Boogaard, A.H., 2016. Influence of ring growth rate on damage development in hot ring rolling. J. Mater. Process. Technol. 227, 268–280.
Zhou, G., Hua, L., Qian, D.S., 2010. FE analysis of coupled thermo-mechanical behaviors in radial-axial rolling of alloy steel large ring. Comput. Mater. Sci. 50 (1), 65–76.